Defence Research and Development Canada | Recherche et développement pour la défense Canada

CAN UNCLASSIFIED

DRDC | RDDC
technologysciencetechnologie

Prediction of Warship Manoeuvring Coefficients using OpenFOAM

Chunhui Liu
Jin Sia
Jean-Pierre Hickey
Department of Mechanical and Mechatronics Engineering, University of Waterloo

Xiaohua Wu
Department of Mechanical and Aerospace Engineering, Royal Military College of Canada

Prepared by:
Department of Mechanical and Mechatronics Engineering, University of Waterloo, 200 University Ave W, Waterloo, Ontario, Canada, N2L 3G1

Department of Mechanical and Aerospace Engineering, Royal Military College of Canada
13 General Crerar Crescent, Kingston, Ontario, Canada, K7K 7B4

Contract Number: PA16004
Technical Authority: Kevin McTaggart, Defence Scientist

Contractor's date of publication: October 2019

Defence Research and Development Canada

Contract Report
DRDC-RDDC-2019-C259
November 2019

Canada

IMPORTANT INFORMATIVE STATEMENTS

This document was reviewed for Controlled Goods by Defence Research and Development Canada using the Schedule to the *Defence Production Act*.

Prediction of Warship Manoeuvring Coefficients using OpenFOAM

Report submitted to:
Dr. Kevin McTaggart, DRDC, Atlantic Research Centre, Dartmouth, Nova Scotia, Canada

Chunhui Liu, Jin Sia, Jean-Pierre Hickey

Department of Mechanical and Mechatronics Engineering, University of Waterloo, Waterloo, Ontario, Canada

Xiaohua Wu

Department of Mechanical and Aerospace Engineering, Royal Military College of Canada, Kingston, Ontario, Canada

Abstract

This report summarizes the results for the static and dynamic planar motion mechanism (PMM) simulations of ship manoeuvring using the open-source Computational Fluid Dynamics software package, OpenFOAM. The well-established DTMB 5415 test case is used to benchmark the static and dynamic PMM simulations. Additionally, the static drift DTC test case is presented as an additional validation case for the predictive force and moment coefficients. The numerical simulations are performed using the InterFoam (for static case) and InterDyMFoam (for dynamic case) packages which are multiphysics CFD solvers based on the volume of fluid (VOF) method to account for the multiple phases in a continuous regime (without needing to track the discrete air-water interface); the turbulence is modelled using Reynolds Averaged Navier Stokes (RANS) approximations. The mesh is non-body conforming and generated via successive mesh refinement and adaptation using open-source software; a dynamic mesh technique is used for dynamic PMM simulations. Despite the lower accuracy of this grid generation method and the mesh deformation in dynamic PMM simulation, the results show an overall good agreement with experimental data and published numerical results. The relative errors remain small–for most of the steady cases under consideration–after a grid convergence study. There are three specific cases in which the error is significant: (1) at a high Froude number; (2) for large steady drift angled (16° and 20° degree cases); (3) for the specific unsteady yaw rate of 0.3 and drift angle of 10° case. In conclusion, OpenFOAM is capable of predicting force and moment coefficients for static and dynamic PMM simulation with a good accuracy outside the three specific cases when the error is non-negligible.

Résumé

Ce rapport résume les résultats de simulations statiques et dynamiques du mécanisme de mouvement planaire (MMP) des manoeuvres d'un navire à l'aide du logiciel OpenFOAM (OpenSource Computational Fluid Dynamics). Le scénario d'essai bien établi DTMB 5415 est utilisé pour étalonner les simulations statiques et dynamiques du MMP. De plus, le scénario d'essai de dérive statique DTC est présenté comme un cas de validation supplémentaire pour les coefficients de force et de moment prédictifs. Les simulations numériques sont effectuées à l'aide des logiciels InterFoam (pour le cas statique) et InterDyMFoam (pour le cas dynamique), qui sont des solveurs CFD multiphysiques basés sur la méthode du volume de fluide (VOF) afin de tenir compte des multiples phases dans un régime continu (sans avoir à suivre l'interface air/eau). La turbulence est modélisée en utilisant des approximations RANS (équations de Navier-Stokes moyennées). Le maillage n'est pas conforme au corps et il est généré par raffinement et adaptation successifs du maillage à l'aide d'un logiciel de source libre. Une technique de maillage dynamique est utilisée pour les simulations MMP dynamiques. Malgré la précision moindre de cette méthode de génération de maillage et la déformation du maillage dans la simulation MMP dynamique, les résultats montrent une bonne concordance globale avec les données expérimentales et les résultats numériques publiés. Après une étude de convergence de maillage, les erreurs relatives restent faibles pour la plupart des cas constants à l'étude. Il y a trois cas spécifiques pour lesquels l'erreur est significative : 1) avec un nombre de Froude élevé, 2) pour les grands angles de dérive stables (16 degrés et 20 degrés), 3) pour une vitesse en lacet instationnaire spécifique de 0,3 et un angle de dérive de 10 degrés. En conclusion, OpenFOAM est capable de prédire les coefficients de force et de moment pour les simulations MMP statique et dynamique avec une bonne précision en dehors des trois cas spécifiques où l'erreur est non négligeable.

Table of Contents

List of Tables

List of Figures

Chapter 1

Introduction

Manoeuvrability is one of the most important performance indicators of ship navigation. There are several ways to estimate the manoeuvrability characteristics of a ship, namely: theoretical approaches, experimental/empirical models and numerically via Computational Fluid Dynamics (CFD). The theoretical approach is limited to slender bodies and does not consider the interaction between the hull and the appendages, nor the more complex non-linear effects. Whereas the theory-based approaches are best suited for order-of-magnitude manoeuvrability approximations. Empirical modelling driven by experimental data is the traditional means for ship maneuverability estimation. This approach typically relies on the measurement of forces and moments on a model ship undergoing static and dynamic planar motion mechanism (PMM) tests. These experimental tests are expensive and time consuming as special experimental platforms are required. Thanks to increasing computational power, CFD is providing researchers with the ability to numerically compute static and dynamic stability derivatives on arbitrarily complex ship geometries. The ship manoeuvring simulations represent a truly multi-physics/multi-scale problem in which many modelling assumptions must be made. As a result of the complexity of the physics, the reliability of CFD represents the main challenge to a broader adoption of this technology. The present work seeks to assess the ability of the open-source CFD package, OpenFOAM (version 17.12 [2]), to accurately compute the forces and moments for ship maneuverability under static and dynamic operating conditions. To assess OpenFOAM's ability to compute ship maneuvers, well-defined test cases with experimental data are se-

lected as benchmarks. In particular, this work deals with static drift, dynamic pure sway, pure yaw, yaw, and drift simulations.

1.1 Sub-scale ship manoeuvring test cases

To assess the predictive ability of Computational Fluid Dynamics solvers for ship manoeuvrability, well-defined experimental test cases must be devised. Of the numerous ship manoeuvring test cases, the US Navy Combatant model 5415 (here denoted as DTMB 5415 [4] as an acronym for the David Taylor Model Basin) provides a well-studied, sub-scale geometry that was used as part of the Workshop on Verification and Validation of Ship Manoeuvring Simulation Methods since the 2000s [24]. This sub-scale ship was inspired by a preliminary design of a US Navy surface combatant ship from the early 1980's. An extensive experimental and parametric database in deep water, including PMM tests, serve as a well-defined benchmark against which numerical tools can be assessed. Other established test cases have also been reported in the literature. Stern [31] presented results for DTMB 5512 in the Iowa Institute of Hydraulic Research (IIHR) towing-tank. Their experimental results include resistance calculations, sinkage and trim, wave profile and nominal wake tests and uncertainty assessment. Similarly, Olivieri *et al.* [37] carried out towing tank experiments for the INSEAN 2340 model (the Italian Ship Model Basin) in the range of Froude number between 0.05 and 0.45 for free model conditions. Comparative assessments between the various international towing-tanks was undertaken by Stern *et al.* [47]. Their work provides a comparative experimental database, at overlapping tests conditions, between three institutes: IIHR, Istituto Nazionale per Studi ed Esperienze di Architettura Navale (INSEAN), and David Taylor Model Basin (DTMB); the results include a detailed uncertainty assessment on the test data from these experiments. A similar uncertainty assessment methodology was presented by Longo [32] for towing tank tests using DTMB 5512.

Of the many types of ship manoeuvring tests that can be conducted, the most common is the static and dynamic planar motion mechanism (PMM) test. Simonsen [46] conducted experiments of pure drift, pure sway, pure yaw, yaw and drift to provide PMM data for comparison with the IIHR towing tank. The 1:35.48 scale model of DDG51 (DTMB5415) was constrained in roll but free to heave and pitch, so trim and sinkage were also obtained. Forces were measured in the longitudinal direction of the ship and perpendicular to this direction. The yaw moment was taken with respect to the mid ship position at the

center between forward perpendicular (Fp) and after perpendicular (Ap). Similarly, Benedetti *et al.* [5] conducted PMM tests for the DTMB 5415 with a scale ratio 1:24.83. Stern *et al.* [54, 55] summarizes the benchmark data for CFD validation; in particular, they consider the force, moment, motion measurements for the DTMB 5512. For free roll motion, Lee *et al.* [26, 27] performed free roll decay tests in calm water with both an intact and damaged ship. These 6DoF motion tests were performed with regular waves for a passenger ship provided by the Ship Safety Research Centre (SSRC) at the University of Strathclyde.

1.2 Ship manoeuvring simulations

International workshops on computational ship hydrodynamics have been held seven times since 1980 in order to standardize testing for naval hydrodynamics. The workshops were held in Gothenburg, Sweden in 1980, 1990, 2000 and 2010 [25], while they were held in Tokyo, Japan in 1994, 2005 and 2015 [3]. Two ship models were used in the first two workshops. The first workshop in 1980 focused on simulation based on simplified boundary layer equations. While most of these simplified methods were capable of predicting ship boundary layer characteristics with reasonable accuracy, they failed in predicting the flow at the stern and in the wake of the vessels. In the second workshop in 1990, most simulations were conducted using Reynolds-Averaged Navier-Stokes (RANS) turbulence closure models. These numerical tools provide a better description of the flow near the propeller plane but still maintain an inaccurate prediction of the bilge vortex. Viscous flow prediction for the Series 60 cargo ship with free surface, multi-phase modelling was added in the workshop in Tokyo, 1994. The Series 60 wave profile was predicted accurately with the RANS simulation, while the damping of the wave pattern was observed due to the insufficient mesh resolution and numerical dissipation.

The increasing availability of computational power resulted in a drastic increase in the number and complexity of the ship models during the 2000 workshop in Gothenburg, Sweden. The simulations included naval hydrodynamics with complex geometries, multi-physics and environment; self-propulsion and the numerical and modelling uncertainties were also presented by participants. Three modern ships were investigated: the KRISO Tanker Ship (KVLCC2), the KRISO Container Ship (KCS), and the U.S. Navy Combatant (DTMB 5415); these ship models have been used ever since. In the fifth workshop in Toyko 2005, seakeeping and manoeuvring cases were shown and the number of test cases increased significantly,

with the same three hulls as in the Gothenburg workshop. The sixth workshop in 2010 covered the areas such as resistance and local flow, self-propulsion and seakeeping with the three previous hull. In the workshop Tokyo 2015, two new hulls were introduced, namely: the Japan bulk carrier (JBC) and the ONR tumblehome ship (ONRT). Besides RANS and DES technique, energy saving devices were presented in the workshop.

1.3 Numerical approaches for ship manoeuvring computations

The Workshop on Verification and Validation has served as the gold standards for the assessment of the predictive ability of numerical simulation for ship maneuverability. These experimental data have been used by a number of researchers to assess the predictive ability of numerical tools. The steady drift cases have been investigated by a number of research groups. Wood et al.[53], using the commercial CFD solver ANSYS-CFX, numerically investigated the steady drift case of the DTMB 5415 with RANS and a free-surface interface modelling approach. Wave profiles, local wave elevations and global resistance were obtained; the comparison between experimental and computational results showed a better prediction by structured mesh than by unstructured mesh. Jones et al. [18] simulated the static drift case for DTMB 5415 using Fluent and noticed that the results were sensitive to the angle of the grid with respect to the free surface waterline. Ma et al. [33] simulated a static drift case for the DTMB 5415 using an in-house CFD code with a level-set method to capture the air-water interface. The total friction and wave profile along the ship were in good agreement with experimental data, although it was noted that a smaller wave on the hull was the result of the dissipation due to the mesh and numerical scheme.

Small-amplitude ship simulation was investigated using the solid-body motion method and dynamic mesh method, which are implemented as open-source tools in the OpenFOAM solver. Vuko et al. [51] investigated pure sway motion for DTMB 5512 and MOERI container ship (KCS) hulls using the OpenFOAM extension: foam-extend. The mesh motion was modelled as rigid body motion and the cells moved at each time step while updating the convective mesh flux. More recently, Islam *et al.* [16] investigated static drift, pure yaw and pure sway motion for KCS by solid body motion solver in OpenFOAM. The predicted forces, yaw moment and hydrodynamic derivatives were compared with the experimental data. The results showed good agreement except for some of the pure yaw cases. Using a dynamic mesh tech-

nique, Henry [39] performed roll decay simulations of DTMB 5415 and DTC hull with a mesh morphing method in OpenFOAM. The 3D forced roll motion was simulated by sliding interface method in OpenFOAM. Commercial tools have also been used for these simulations. Oldfield *et al.* [36] presented static drift, PMM and rotating arm simulation result for DTMB 5415 using STAR-CCM+. Shen *et al.* [43] investigated added resistance, heave and pitch motions of a DTMB 5512 in head waves. The wave is generated by setting a time dependent inlet boundary condition, and a sponge layer is setup at the outlet of the computational domain to avoid wave reflection; 6DoF motion is captured by a dynamic mesh. The simulation result was validated by experiment data [11, 12, 15].

For ship simulation with large amplitude motion, the overset method is generally the preferred approach. Sakmoto *et al.* [41] verified and validated the forces and moment coefficients, and hydrodynamic derivatives in static and dynamic PMM simulation for DTMB 5415 using the in house code CFDShip-Iowa. This code is an URANS solver with overset grid technique to deal with dynamic ship motions and local grid refinements. Carrica *et al.* [6] investigated steady turn and zig-zag motions for DTMB 5415 using a hierarchy of body technique. More recently, Shen [45] developed a dynamic overset grid within OpenFOAM (although not publicly available) and performed simulation of zig-zag motions with self-propulsion for a full dynamic simulation case.

A second well-established ship manoeuvring case is the Duisburg Test Case (DTC), which is used as a benchmark case for modern container vessels. Although not a military ship, this case provides a secondary validation case on the force estimates and is receiving increasing attention for benchmarking CFD solvers. For this case, el Moctar *et al.* [8] presented both experimental and numerical simulation data for the DTC model with resistance test and roll decay test. Kinaci *et al.* [23] researched ship propeller interaction problem of DTC by numerical simulation whereas Liu *et al.* [30] presented a three-dimensional nonlinear time domain method for the simulation of six-degrees of freedom (DoF) motion of the case. In the same year, Ley *et al.* [28] predicted the added resistance of the DTC in waves using the commercial software Comet and the open-source alternative OpenFOAM. More recently, el Moctar *et al.* [9] further investigated the effects of waves on manoeuvring using both experiments and CFD. The full-nonlinear effects were investigated by He *et al.* [13] who impemented an overset grid for a three-degree of freedom simulation, which is capable of simulating larger ship movements as well as the bottom hull interaction for DTC. Recently, Terziev *et al.* [49] investigated the behavior of trim, sinkage and resistance for DTC in shallow waters at varying channel cross-sections and speeds. The numerical simulation results by Star-

CCM+ were compared to those by slender body theory and it showed good agreement in the low speed range.

In Table 1.1, a comprehensive summary of the known CFD software used for ship manoeuvring simulations is presented as an overview.

1.4 Objective of present work

An objective of this work is to validate OpenFOAM as a reliable tool to estimate ship manoeuvring forces and moment coefficients. It should be noted that in addition to the main CFD solver, all the pre- and post-processing tools are open-source tools; this includes the mesh generation and visualization of the data (e.g. snappyHexMesh, Python, VisIt, Paraview). Static drift and unsteady pure sway, pure yaw, yaw and drift simulations for DTMB 5415 are compared to the model test data [37, 46]. Although the primary reference case is the DTMB 5415, we chose to additionally study static drift DTC case [8] as an additional validation on a different geometry using the same open-source software package. Unsteady PMM simulations of DTMB 5415 are performed by dynamic mesh technique [17], in which the ship motion is prescribed in advance and the mesh is deformed without topological changes. This report is organized as follows. In chapter 2, numerical details about OpenFOAM solver and ship models are presented. The validation of DTC and DTMB 5415 is discussed in chapter 3 and relative error analysis is proposed by comparison with model test. In chapter 4, a final summary and discussion is given.

Software	**Type**	**Numerical techniques**	**Relevant literature**
OpenFOAM	open source	FVM, VOF, URANS	[16], [28], [39], [51]
naoe-Foam-SJTU	inhouse	waves, overset, 6DoF; self propulsion, PMM	[42], [45], [43], [52]
Navy-Foam	inhouse	waves, overset, 6DoF	[10], [22], [21]
CFDShip-Iowa	inhouse	URANS, level set, waves, overset, 6DoF	[6], [41]
ShipMotion	inhouse	URANS, density function [19],overset,FVM	[20]
WISDAM-X	inhouse	URANS, density function [19],waves,overset,FVM	[38]
ANSYS-CFX	commercial	URANS, VOF	[53]
Fluent	commercial	URANS, VOF	[18]
Star-CCM+	commercial	URANS, VOF	[36]
Comet	commercial	URANS, VOF	[28]

Table 1.1: Summary of CFD software for ship manoeuvring simulations.

Chapter 2

Numerical details

2.1 Mathematical model

The numerical simulations have been carried out using OpenFOAM (version 17.12 [2]), an open source multi-physics fluid solver. Three-dimensional incompressible Navier-Stokes equations in a multi-phase framework are discretized and solved by finite volume method (FVM). The turbulence is modelled using a variety of conventional steady and unsteady RANS models. A Volume-Of-Fluid (VOF) method [14] is used to model the multiple phases within the domain. The VOF method does not explicitly track the phase interface, but instead it assumes a continuum in each cell; in other words, each cell consists of a given volume of water, air, or solid in our current setup and the aggregate properties of the cell are computed based on the fraction of each phase. The pressure and velocity are decoupled by the PIMPLE algorithm which is a combination of a classical PISO (Pressure Implicit with Splitting of Operator) and SIMPLE (Semi-Implicit Method for Pressure-Linked Equations) schemes. For the current simulations, the turbulent flow is modeled by $k\omega - SST$ model [35]. The simulations were conducted at the kinematic viscosity of water $\nu_w = 1.09 \times 10^{-6} m^2/s$, water density $\rho_w = 9.988 \times 10^2 kg/m^3$. For the gaseous portion of the domain, the kinematic viscosity of air $\nu_a = 1.48 \times 10^{-5} m^2/s$, density $\rho_a = 1 kg/m^3$ are used.

For static simulations, the InterFoam solver is used, with an implicit first-order Euler scheme for pseudo-time integration; for steady-state simulations, this low-order pseudo-time integration is satisfactory. For

unsteady cases (pure sway, pure yaw,yaw and drift motion), the interDyMFoam solver is used with dynamic deforming mesh [17]. The mesh deforms based on the movement of the ship, without topological change. The displacement of mesh point is calculated by solving the following Laplace equation at each time step:

$$\nabla.(\gamma \nabla x_g) = 0 \tag{2.1}$$

where x_g is movement of mesh point; γ is the diffusivity coefficients based on the square inverse of distance between the ship and mesh point. First order implicit Euler scheme is used for time integration.

2.2 Coordinate system and non-dimensionalization

For ship manoeuvring simulations, there are two coordinate systems of interest: the earth coordinate system and the ship-fixed coordinate system. Both coordinate systems follow the right-hand rule, as shown in Figure 2.1. In ship fixed coordinate, the x-axis is positive from the stern to the bow and the z-axis is positive upwards. The origin of the earth coordinate system is generally located at the start point of manoeuvring simulation, while the origin of the ship-fixed coordinate is taken with respect to the mid-ship position at $L_{pp}/2$. Drift angle β is the horizontal angle between the x-axis of the ship and the tangent to its path. All results in the current simulations are reported in the ship coordinate system. The forward velocity u, sway velocity v, and clockwise angular velocity r are non-dimensionalized by the magnitude of ship velocity U and the ship length between perpendiculars L_{pp}:

$$u' = \frac{u}{U}, \qquad v' = \frac{v}{U}, \qquad r' = \frac{rL_{pp}}{U} \tag{2.2}$$

The forces and moment are non-dimensionalized as follows:

$$X' = \frac{X}{0.5\rho U^2 L_{pp} T_m}, \qquad Y' = \frac{Y}{0.5\rho U^2 L_{pp} T_m}, \qquad N' = \frac{N}{0.5\rho U^2 L_{pp}^2 T_m} \tag{2.3}$$

where T_m[m] is the mid-ship draught, and ρ [kg/m^3] is the density of water.

2.3 Domain definition and boundary conditions

The computation domain is shown in Figure 2.2, where the blue region represents air and red region represents water. A deep water condition is represented in the current domain. For all cases, a full

domain is selected even in the cases where a symmetry plane can be defined. Seven patches are defined as boundaries in the current simulation: inlet, outlet, bottom, atmosphere, front, back and the hull, where front patch is defined at the starboard side and back patch is defined at port side of the hull. The boundary condition at the inlet, outlet and atmosphere are defined based on the velocity of the ship. A no-slip wall boundary condition is used on the hull in both the water and air. The boundary condition of the bottom is set as symmetry plane. The boundary conditions on the front and back are defined based on the drift angle in the simulation, as shown in Figure 2.3. For cases $drift = 0°$, symmetry boundary condition is set on both of the front and back patches; for cases with a non-zero drift angle, the velocity inlet boundary condition is defined for the back patch, the outlet boundary condition is defined for front plane. The inlet flow velocity is parallel to the center plane of the domain in cases of $drift = 0°$, while the angle between inlet flow velocity and center plane of domain equals to drift angle in cases $drift \neq 0°$. The current method to deal with drift cases can improve the accuracy of the simulation, compared to the method that rotating the hull model since the mesh quality would decrease with the rotation of hull. These aspects will be discussed in section 2.5.

The detailed information about the boundary conditions of the simulations and turbulent parameters is presented in the Table 2.1. FV representes a fixed value, which is a first-type boundary condition (Dirichlet); the boundary value for the variable is explicitly prescribed. ZG is zero-gradient (second-type boundary condition, Neumann); PIOV is the pressure-inlet/outlet velocity. MWV is the moving wall velocity, which is set as a fixed type zero in static simulation and a calculated type in dynamic simulations. FFP is an abbreviation for fixed-flux pressure, which adjusts the pressure gradient to match the velocity boundary condition while TP is the total pressure. VHFR represents variable height flow rate, providing a phase fraction condition based on the local flow conditions. IO is inlet and outlet boundary; it provides zero gradient outflow conditions normally while it switches to fixed value if there is back flow, as shown in the Figure 2.4. kqRWF is the wall function for turbulent kinetic energy and nutkRWF is the rough wall function for turbulence kinetic eddy viscosity ν_t. omegaWF is the wall function for specific rate of dissipation. The boundary condition of pointDisplacement is only prescribed in the dynamic cases, where MWD represent a moving wall displacement defined by user for specific type of motion.

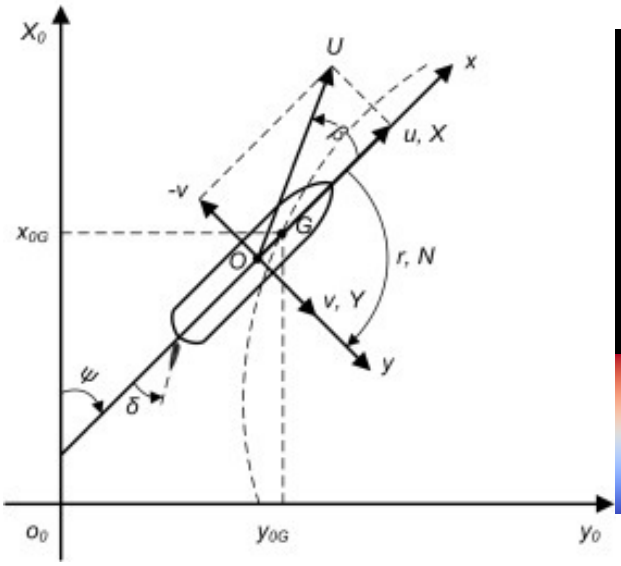

Figure 2.1: Coordinate system [29].

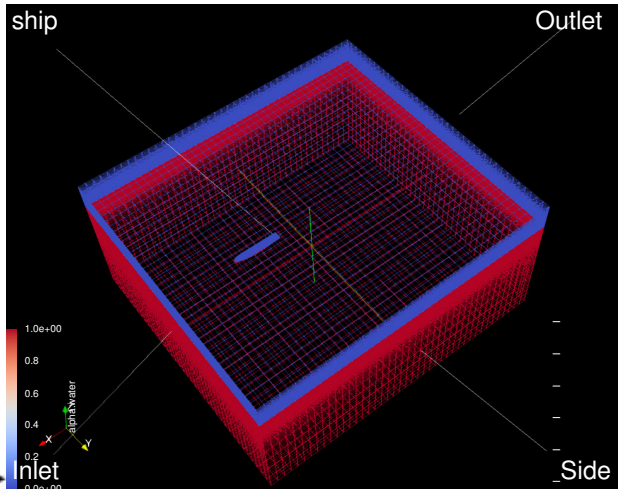

Figure 2.2: Computation domain and boundaries.

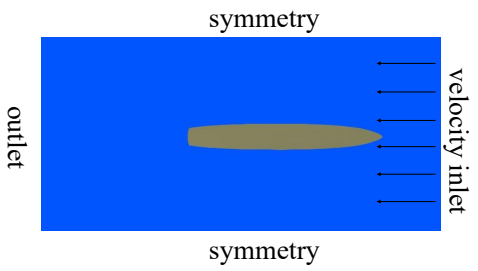

(a) $drift = 0°$

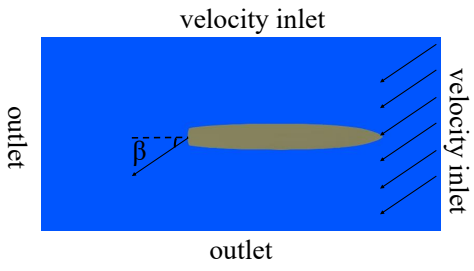

(b) $drift = \beta$

Figure 2.3: Boundary condition for inlet, outlet, front, and back.

	Inlet	Outlet	Atmosphere	Ship
U	FV	ZG	PIOV	MWV
p_{rgh}	FFP	ZG	TP	FFP
alpha.water	FV	VHFR	IO	ZG
k	FV	IO	IO	kqRWF
nut	FV	ZG	ZG	nutkRWF
omega	FV	IO	IO	omegaWF
pointDisplacement	FV	FV	FV	MWD

Table 2.1: Boundary condition for fluid and turbulence parameters.

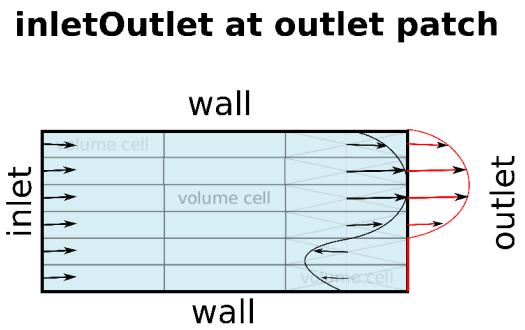

Figure 2.4: InletOutlet boundary condition. Source [1]

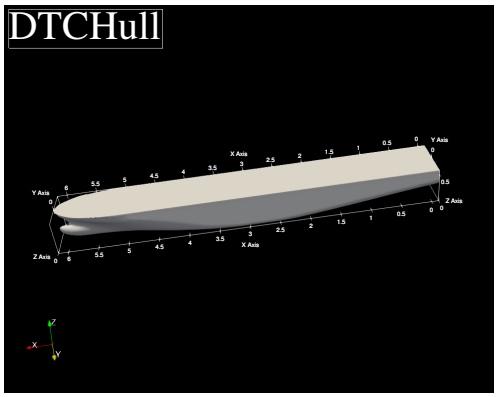

(a) DTC

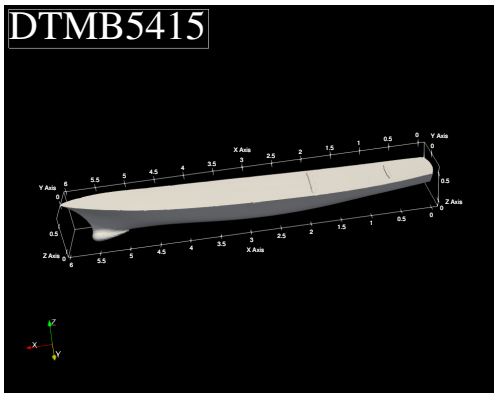

(b) DTMB 5415

Figure 2.5: The geometry of the ship model.

2.4 Ship model

The ship models used for benchmarking OpenFOAM are, as previously discussed, the DTC and DTMB 5415, as shown in Figure 2.5. The geometric files defining the outer hull of the vessels are available on the website of the Workshop on Verification and Validation of Ship Manoeuvring Simulation Methods. The main parameters of the DTC and DTMB 5415 are presented in Table 2.2 and Table 2.3 respectively, where B_{wl} is waterline breadth, T_m is midship draught, V is volume displacement, C_B is block coefficient, S_w is wetted surface under rest waterline without appendages and V_d is design speed. The DTMB 5415 model does not include bilge keels in the current simulations. Sinkage and trim are set based on the experimental data [46] in the current simulations.

2.5 Computational mesh

Two types of mesh are generated by snappyHexMesh utility in OpenFOAM in the current simulation: a coarse mesh and a high-resolution mesh. The coarse mesh for DTMB 5415 is shown in Figure 2.6 and the high-resolution mesh is shown Figure 2.7. For the coarse mesh, we selected the computational domain to be L_x,L_y,L_z=42, 38, 20 for a unitary ship size. For the high resolution mesh, we selected a smaller

DTC	$Model$	$FullScale$
$L_{pp}[m]$	5.976	355.0
$B_{wl}[m]$	0.859	51.0
$T_m[m]$	0.244	14.5
$\vartheta[^\circ]$	0.0	0.0
$V[m^3]$	0.827	173467.0
C_B[-]	0.661	0.661
$S_w[m^2]$	6.243	22032.0
V_d[knots]	3.244	25.0

Table 2.2: Main parameters for DTC.

$DTMB5415$	$INSEAN$	$MARIN$
Scale ratio	24.83	35.48
$L_{pp}[m]$	5.72	4.002
$L_{wl}[m]$	5.726	4.0083
$T_m[m]$	0.248	0.173
C_B[-]	0.5060	0.507

Table 2.3: Main parameters for DTMB 5415.

computational domain with L_x,L_y,L_z=40, 18, 9, which also satisfies the ITTC guidelines [40]. In the first step, a multi-grading functionality is used in blockMesh to generate background mesh: where a gradual refinement in three direction is achieved, with uniform refined three-dimensional mesh near the hull. In the second step, refineRegion and refineSurface functionality in the SnappyHexMesh tool are successively used, each refinement level splits the cell size in half over the defined air-water interface region and the region near the hull surface.

2.6 Motion

Different types of motions in the current CFD simulations are presented in Figure 2.8. The carriage speed U is fixed based on Froude number. For steady drift simulations, the drift angle β and carriage speed were specified from 0° to 20°. The velocity in ship coordinate reduces to $u = Ucos\beta$, $v = Usin\beta$. For unsteady PMM simulations, the motions were set by the PMM model tests in the experiment [46].

2.7 Computational resources

The simulations were performed on the Niagara supercomputer at the SciNet HPC Consortium with 40 cores, a clock speed of 2.4 GHz and 202 GB of Random Access Memory (RAM). The wall clock time was approximately 3000s per static simulation. The static simulations were run up to 4000s with a time step of 1s for attaining converged results. In the dynamic cases, the wall clock time was approximately 20 hours per simulation, with an average time step of 0.001s and simulation time of 20s to obtain stable results.

(a) whole domain

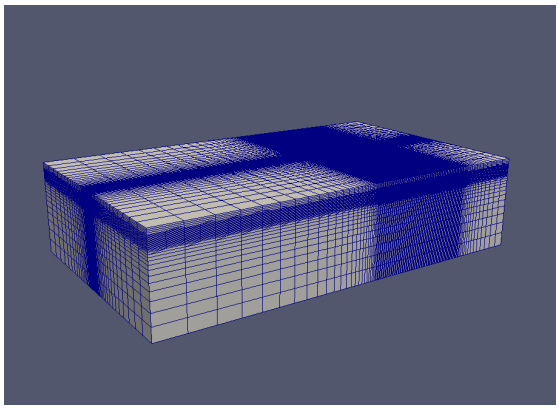

(b) DTMB 5415

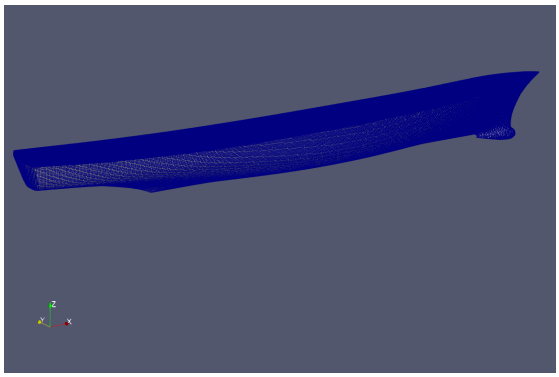

(c) center plane: enlarged rear

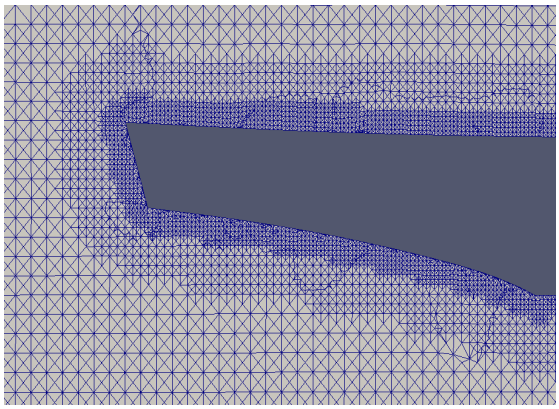

(d) center plane: enlarged front

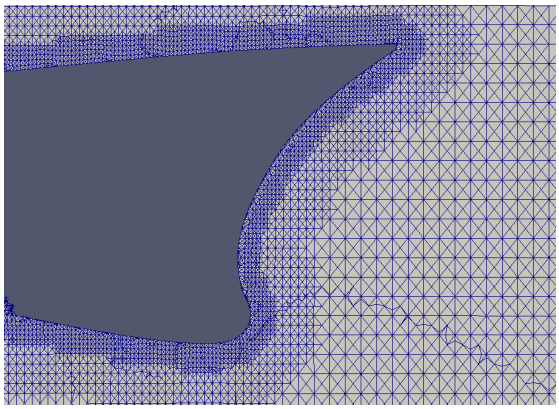

(e) top view: enlarged rear

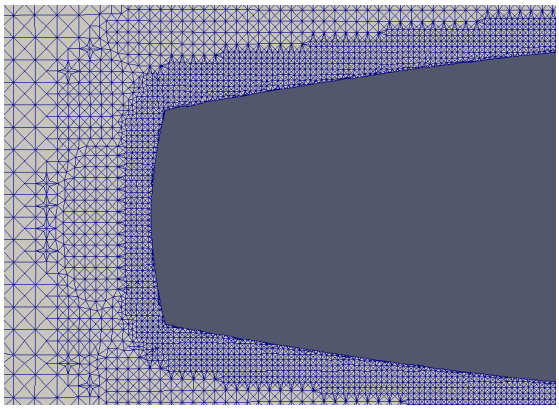

(f) top view: enlarged front

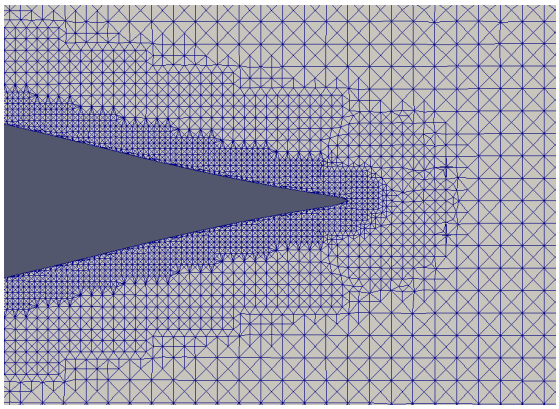

Figure 2.6: Mesh for DTMB 5415 by refineSurface (number of grid points: 2.37 million).

(a) whole domain

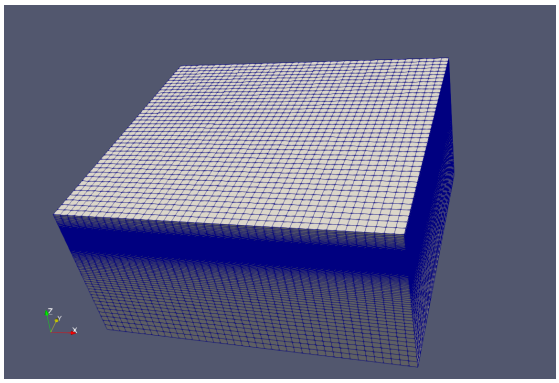

(b) DTMB 5415

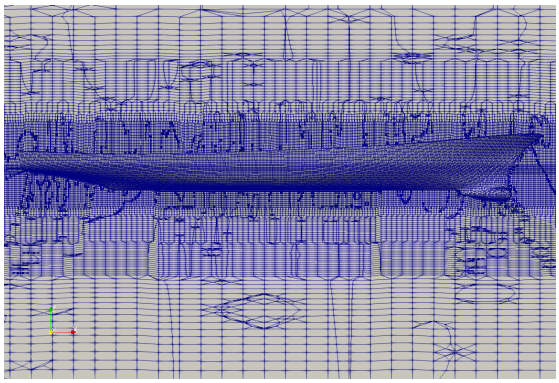

(c) center plane: enlarged rear

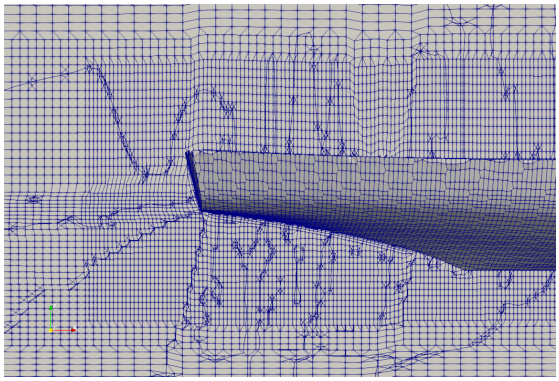

(d) center plane: enlarged front

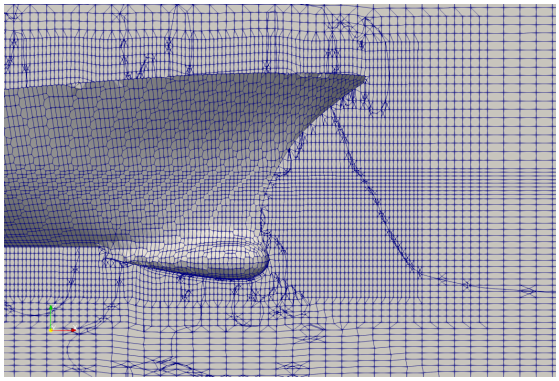

(e) top view: enlarged rear

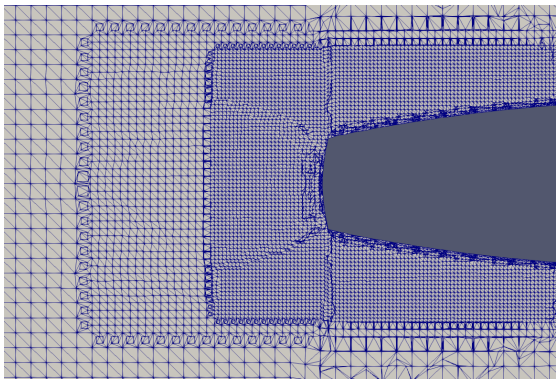

(f) top view: enlarged front

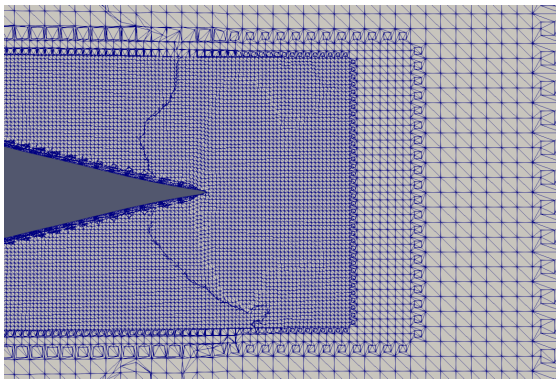

Figure 2.7: Mesh for DTMB 5415 by topoSet (number of grid points: 2.99 million).

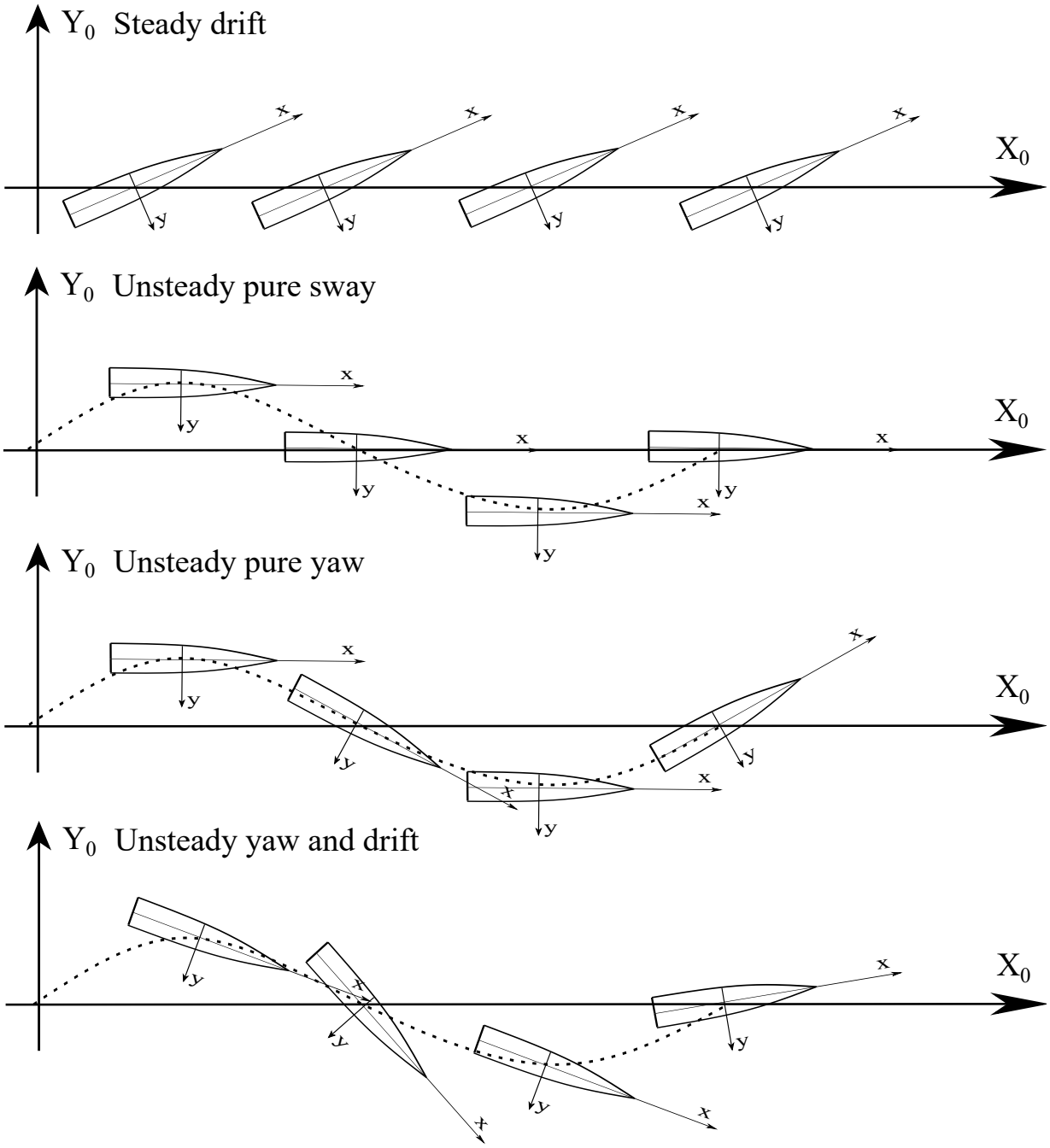

Figure 2.8: Ship motions for simulation of PMM tests.

Chapter 3

Results

This report focuses on the steady and unsteady PMM simulation. All test cases are summarized in Table 3.1. A mesh-independence study was performed with five different resolution for both the DTC and DTMB 5415 at drift 0°. Different Froude number simulations were conducted at drift angle of 0° for validation of both the DTC and DTMB 5415. Further steady and unsteady PMM cases at $Fr = 0.28$ (for DTMB 5415) were investigated. From the resulting numerical simulations, drag, lateral force, and yaw moments were calculated and compared against experimental data. The animations of the mesh movement and hydrodynamic pressure distribution in dynamic PMM simulation is presented in https://www.youtube.com/channel/UCKjJx2ACHCDmguEGGf6eEKQ.

3.1 DTC test case

3.1.1 Verification

Mesh-independence study was performed at $Fr = 0.218$. The different meshes for the DTC case are presented in Figure 3.1, where $m2$ means twice the grid refinement near the hull and $m5$ five times refinement near the hull. For different mesh resolutions, the first layer distance to the hull, the total

Cases	**Conditions**	**Grid**	**Solver**
Static drift: DTC	$\beta = 0°, Fr \in [0.174, 0.218]$	topoSet	interFoam
Static drift: DTMB 5415(INSEAN)	$\beta = 0°, Fr \in [0.05, 0.45]$	topoSet	interFoam
Static drift: DTMB 5415(MARIN)	$\beta \in [0°, 20°], Fr = 0.28$	refineSurface	interFoam
Pure sway: DTMB 5415(MARIN)	$\beta = 0°, Fr = 0.28$	refineSurface	interDyMFoam
Pure yaw: DTMB 5415(MARIN)	$\beta = 0°, Fr = 0.28$	topoSet	interDyMFoam
Yaw and drift: DTMB 5415(MARIN)	$\beta = 10°, Fr = 0.28$	topoSet	interDyMFoam

Table 3.1: Test cases for the static and dynamic PMM simulations.

Mesh	$m2$	$m3$	$m4$	$m5$	$m6$
number of grid points [10^6]	0.668	0.913	1.260	1.718	2.679
first layer distance [m]	0.25	0.125	0.015	0.015	0.005
relative error [%]	54	-18	0.87	-3.3	-0.56

Table 3.2: Grid independence study on the resistance coefficient of DTC (Fr=0.218, drift=0°).

number of mesh points, and convergence of the relative error of resistance coefficient, compared with model test data [8] are shown in Table 3.2. The non-dimensional distance of the first layer from the hull, y^+, equals 280 for the finest mesh $m6$ which is slightly superior to the suggested value of 100 for the use of wall models. We consider this value to be acceptable and consistent with the current wall function used in conjunction with the turbulence models used in OpenFOAM.

3.1.2 Validation

With varying Froude numbers between 0.174 to 0.210 on the finest mesh, the relative error on resistance coefficient is tabulated in Table 3.3. The visual comparison of the resistance force with the experimental data over a range of Froude numbers is shown in Figure **??**. The results provide evidence of a good agreement for the predictive numerical simulations with the experiments for the DTC case.

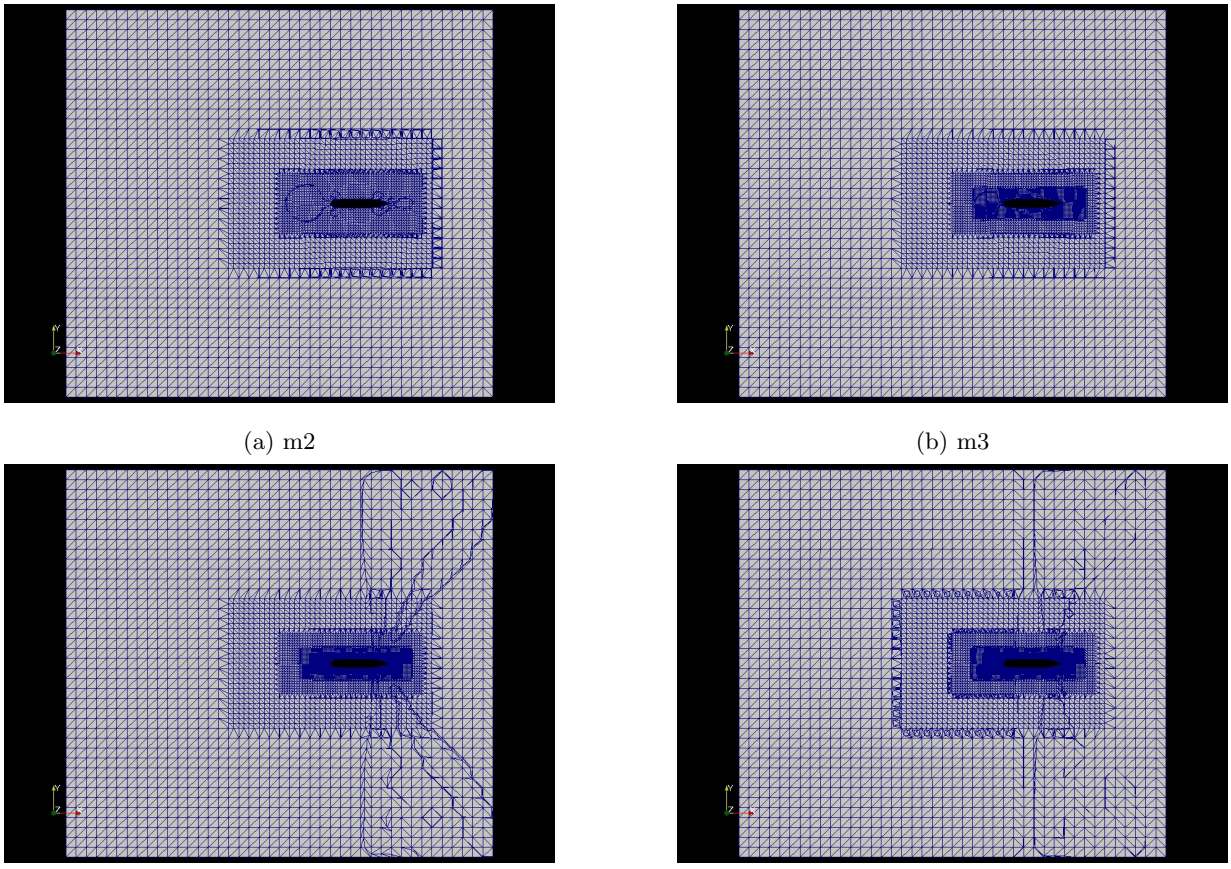

(a) m2

(b) m3

(c) m4

(d) m5

Figure 3.1: Grid independence study for DTC at drift 0°.

Fr	0.174	0.183	0.192	0.200	0.210	0.218
relative error [%]	0.64	0.03	0.67	0.34	1.6	0.56

Table 3.3: Resistance coefficient for DTC at different Froude numbers, drift 0°.

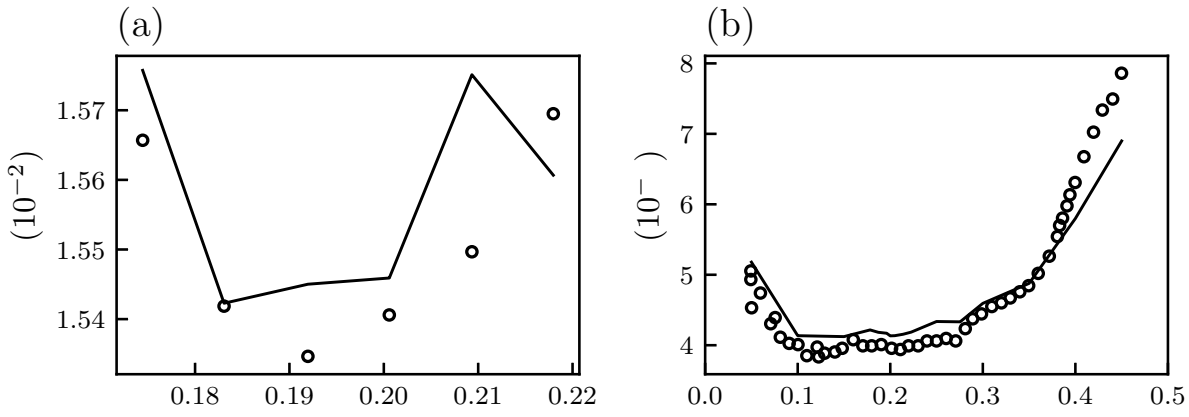

Figure 3.2: Resistance coefficients at drift 0°. ○ Experimental data, '-' OpenFOAM.

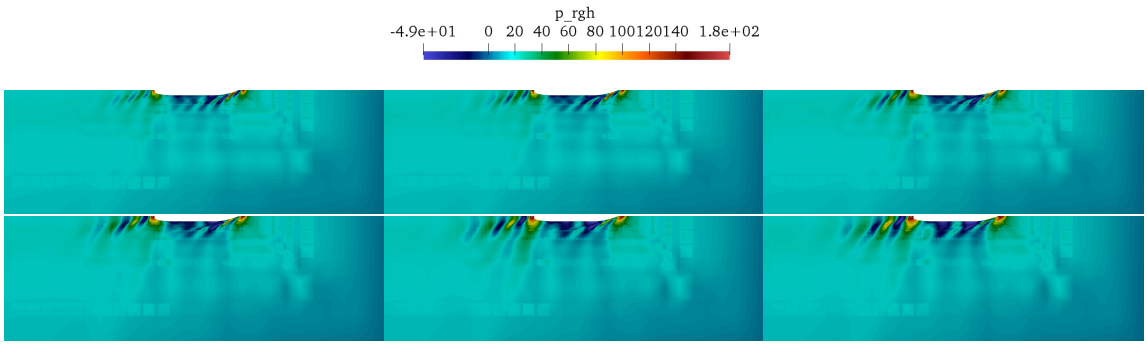

Figure 3.3: DTC: Hydrodynamic pressure distribution on the free surface at Fr= 0.174, 0.183, 0.192, 0.200, 0.210, 0.218 (from upper left to bottom right).

mesh	m2	m3	$m4$	$m5$	$m6$	refineSurface
number of grid points [10^6]	0.669	0.916	1.273	1.778	2.995	2.37
first layer distance [m]	0.25	0.125	0.015	0.015	0.005	0.0125
relative error [%]	49.6	14.0	28.3	1.21	4.13	3.04

Table 3.4: Resistance coefficient of DTMB 5415 (Fr=0.28, drift=0°) for different mesh resolutions.

3.2 DTMB 5415 case

3.2.1 Verification

For the DTMB 5415 case, mesh-independence study was performed at $Fr = 0.28$ and drift angle of 0° which allows us to compare with the experimental data taken from [37]. Similar as mesh-independence test for the DTC, different refinement levels from $m2$ to $m6$ near the hull were used as a criteria for the different mesh resolutions. The non-dimensional distance of first grid layer from the hull y^+ equals 280 for the finest mesh: $m6$. The number of grid points, first layer distance to the hull, and relative error on the resistance coefficient in different mesh resolution is shown in Table 3.4. As the error is less than 4.13%, we deem the mesh resolution $m6$ refined by topoSet method and the mesh refined by refineSurface method to be accepTable for the parametric study.

3.2.2 Validation: $drift = 0°$, $Fr = 0.28$

The comparison of the free wave height around the ship hull (at $Fr = 0.28$) with published data from the open literature is shown in Figure 3.4; Figure 3.5 shows the experimental results [37]. The OpenFOAM results are consistent with both published experimental and numerical simulations, which supports the claim that the VOF method can capture the wave near the hull. Despite the overall good agreement, we do note that there is dissipation of the wave height due to the mesh stretching at the interface–this is especially true away from the ship hull. The air-water interface on the ship hull is shown in Figure 3.6. The trend of the wave height computed from CFD is consistent with the experimental results, but again

we do note a slightly lower peak (0.17) in the simulation compared to experiment (0.18). Over the entire ship length, the wave height is slightly over-predicted. The cause of difference stems from limited mesh resolution in this region of the ship hull. Wave profile away from the ship at $y/L_{pp} = 0.082, 0.172, 0.301$ is also presented and compared with experimental data. At $y/L_{pp} = 0.082$, strong non-physical oscillations near the hull are observed in the simulation, which may due to the stretch ratio of mesh refinement near the hull. At $y/L_{pp} = 0.172$ and $y/L_{pp} = 0.301$, the wave trend is consistent with the experiment. The phase error of the wave at $y/L_{pp} = 0.301$ may result from the dispersion of the numerical scheme.

The wake of the paddle disk is important for the propeller design as it influences the propulsion efficiency. The correct prediction of the wake is critical for predictive ship manoeuvring simulations. Figure 3.7a presents the streamwise velocity contour between experimental data (left) and numerical simulation (right); the simulations were done using an overset method as described by Shen [45]. The current simulation results are shown in Figure 3.7b and are consistent with both experimental and numerical results from the open literature. Due to the presence of spanwise vortices, the contours of the streamwise velocity show humps away from the hull. The current simulation can capture key characteristic of the wake near stern, which is useful for propeller design.

3.2.3 Validation: resistance at different Froude numbers, drift 0°

We vary the Froude number of the simulations between 0.05 to 0.45;Table 3.5 shows the relative difference between model test and numerical simulation results. The relative error is smaller than 6.55% at Fr ranging from 0.05 to 0.4 and it reaches 12.5% at $Fr = 0.45$. As the Froude number increases, magnitude of the error on the resistance coefficient in numerical simulation increases, probably due to a lack of mesh resolution at higher Froude numbers. The comparison with experimentally determined values is shown in Figure **??** and reveals an overall good agreement of the predictive simulations–especially to capture the trends.

3.2.4 Validation: pure drift

Pure drift simulations (recall Figure 2.8) were conducted at different drift angle β from 0 to 20 degrees and at a Froude number of 0.28. The relative error of the forces and drift moments are tabulated in Table

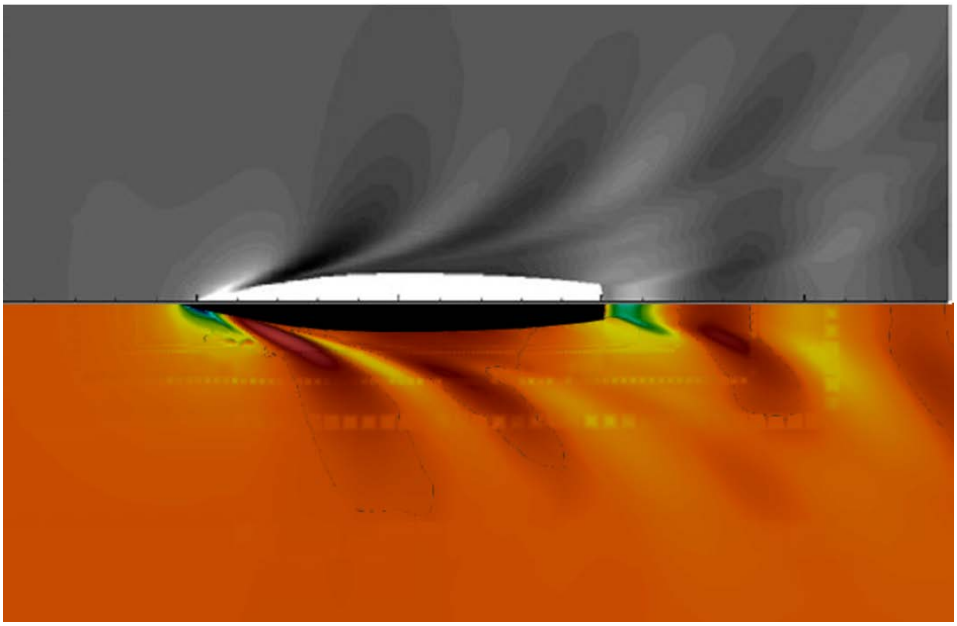

Figure 3.4: Comparison of the free surface wave height of the numerical simulations by Ma [33] (top half) and the OpenFOAM results of the present simulation (bottom half).

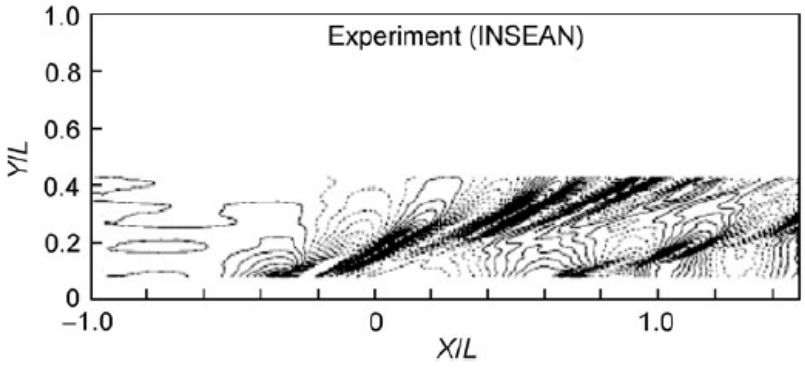

Figure 3.5: Free surface wave height from the experimental results by Oliveri [37] on the DTMB 5415 case.

Fr	0.05	0.1	0.15	0.2	0.25	0.28	0.3	0.35	0.4	0.45
relative error [%]	4.84	2.87	4.36	4.63	6.55	4.13	3.24	0.782	-5.68	-12.1

Table 3.5: Relative error of resistance coefficient for DTMB 5415, at drift 0°.

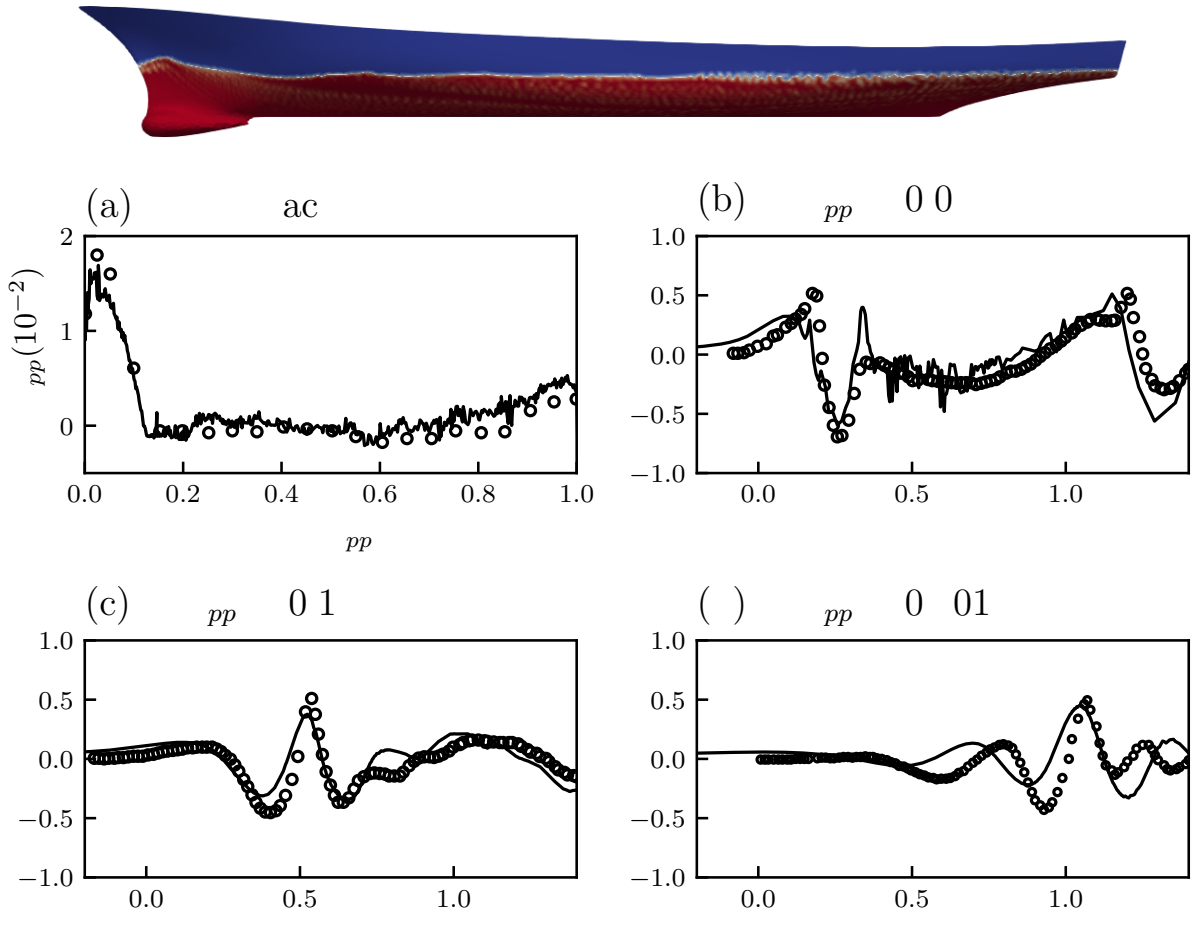

Figure 3.6: Wave on DTMB 5415 ship surface, Fr=0.28, drift=0°. ∘ Experimental data; − OpenFOAM.

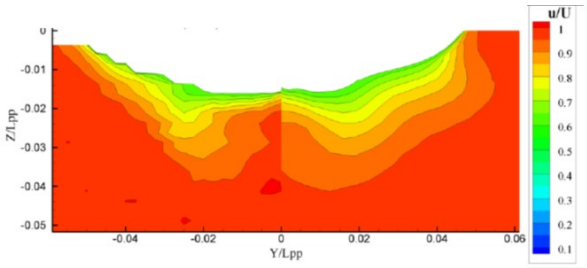

(a) Left: experimental result; Right: numerical simulation [42].

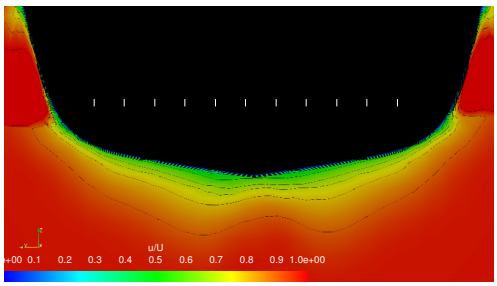

(b) OpenFOAM

Figure 3.7: Streamwise velocity contour of the paddle disk.

3.6, the numerical predictions of the coefficients are compared with experimental data [46]. The current simulation results match well with the experimental data. The only exception is the resistance coefficient X' at drift angles of 16° and 20°. The relative error is shown in Table 3.6. For X', the relative error are smaller than 6% at drift angle range from $\beta = 0°$ to $\beta = 12°$; while it reaches 16% at $\beta = 16°$ and 25% at $\beta = 20°$. The prediction of forces and moment coefficient with different drift angles is presented in Figure 3.8 and shows the overall good trend with increasing drift angles.

Furthermore, the hydrodynamic pressure distribution on the free surface at different drift angles is shown in Figure 3.9. The pattern of hydrodynamic pressure shows stronger asymmetry due to the larger drift angles. The pressure shows an expected strong asymmetry and there are strong pressure fluctuations in the starboard side as the drift angle increases. The pressure pattern is not well-resolved at the high drift angles as the same mesh is used in all drift simulations. This may lead to some errors in the force and moment coefficients. In addition, these error may be compounded by the under-estimation of wave height on the ship surface.

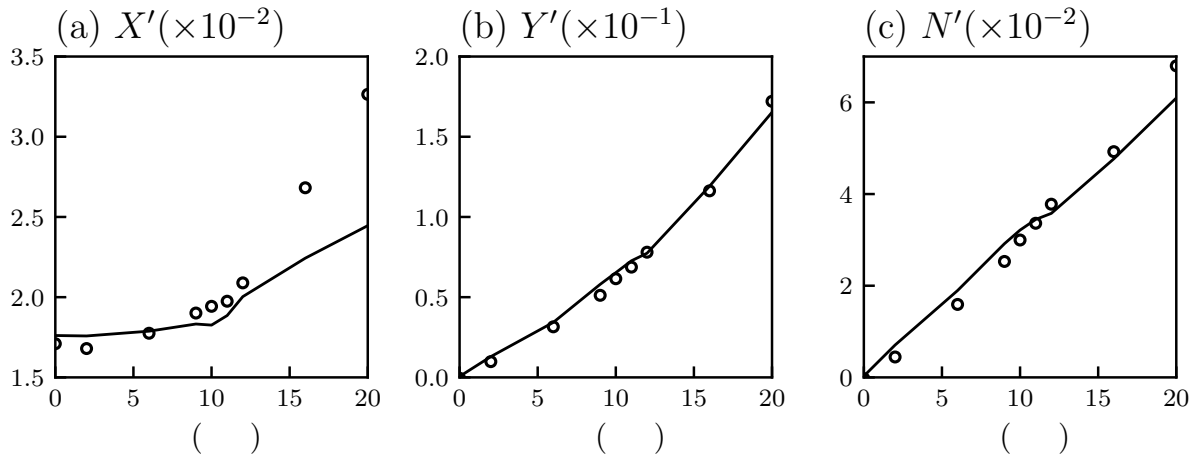

Figure 3.8: Forces and moment coefficient for static drift at different drift angles. ∘ Experimental data; − OpenFOAM.

Drift angle(°)	0	2	6	9	10	11	12	16	20
X'	3	4.7	0.73	3.6	6.0	4.5	4.1	16	25
Y'	-	3.2	8.8	13	6.1	5.7	0.81	2.5	4.0
N'	-	59	19	15	7.2	2.5	5.3	3.2	10

Table 3.6: Relative error(%) of forces and moment coefficients at different drift angles.

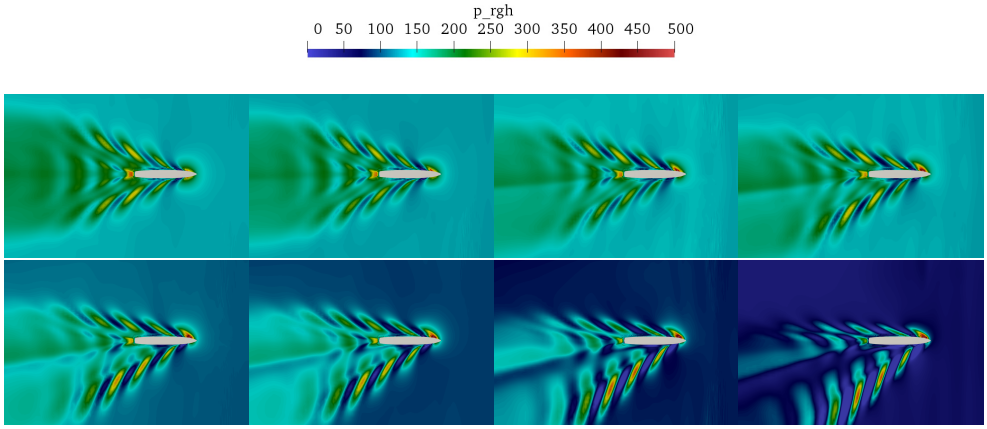

Figure 3.9: Hydrodynamic pressure distribution on the free surface at static drift 0°, 2°, 6°, 9°, 11°, 12°, 16°, 20° (from upper left to bottom right)

3.2.5 Validation: pure sway

The time evolution of the force and yaw moment coefficients are shown in Figure 3.10. The pure sway is defined as $y = Asin(\omega t)$ where $\omega = 0.733 rad/s$, and $A = 0.4158m$. The Figure 3.10 shows that, although there are some deviations in the resistance coefficient X' and lateral force coefficient Y' between the CFD and experimental data, the CFD results follow the trend of the experimental data. This is especially true for the yaw moment coefficient. A lack of refinement near the wake due to the sway motion may lead to the error. Figure 3.11 shows the pressure distribution at the waterline plane. The sway motion induced different pressure distributions on the hull for port and starboard side.

3.2.6 Validation: pure yaw

During the pure yaw motion, the ship axis is tangent to its path. Yaw motion is applied directly to the ship hull, while restricting all other motion. The yaw motion was performed by coupling of oscillatingDisplacement and angularOscillatingDisplacement, using fvMotionSolver in the dynamicMeshdict. The motion is defined as:

$$\begin{aligned} y = y_{max} sin(\omega t) \qquad & \text{where } \omega = 0.733 \text{ rad/s}, y_{max} = 0.4158 \text{ m} \\ \theta = \theta_{max} sin(\omega t) \qquad & \text{where } \theta_{max} = 0.4179467 \text{ rad} \end{aligned} \tag{3.1}$$

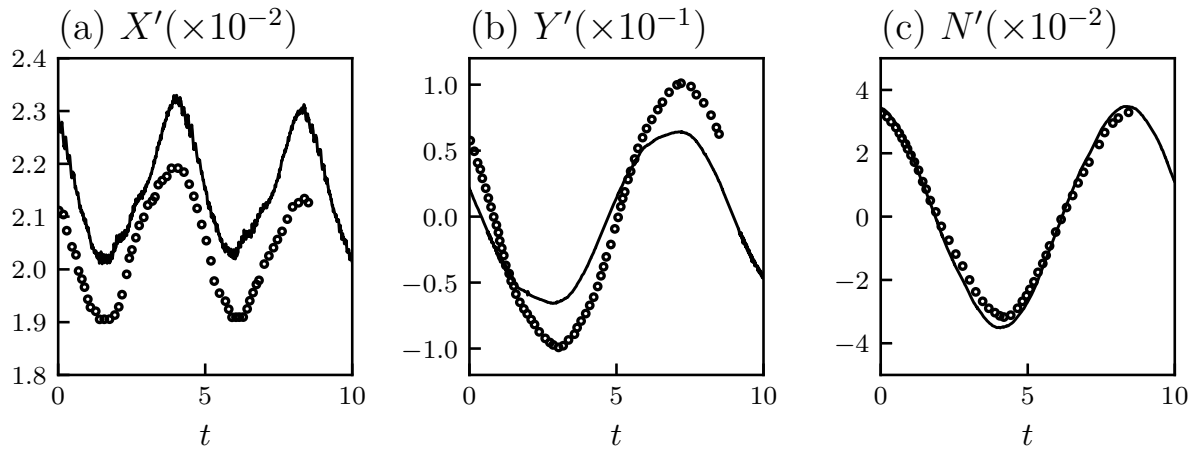

Figure 3.10: Forces and moment coefficient for pure sway.

In the pure yaw case, there is a phase shift between the yaw angle and lateral motion, as presented in the Figure **??**. The lateral motion is maximum when the yaw angle equals zero and vice versa. Lateral motion is set to 0 in the first quarter of period to ensure gradual positioning of the ship.

The time evolution of forces and yaw moment coefficient are shown in Figure 3.12. The simulation results were compared with experimental data by Simonsen [46]. The time history of forces and yaw moment in CFD capture the trend of experimental data; however the amplitude of lateral force in CFD is under predicted, since we chose coarse mesh in the pure yaw simulation for numerical stability.

3.2.7 Validation: yaw and drift

In the case of a yaw rate of 0.3 and a drift of 10 degrees, the motion of the ship is the same as the pure yaw motion in the current simulation. The drift angle is prescribed by the angle of attack between the inlet flow and the inlet boundary, which is the same as the method used in the pure drift simulation. The mesh in the yaw and drift case is the same as that in the pure yaw simulation. A large deviation of forces and moment coefficient is observed between the CFD and experimental data, as presented in Figure 3.14. The deviation may result from the following: (1) the coarse mesh resolution close to the hull, near the wave surface, in the region of the wake; (2) the k-omega-SST model with the wall function, which may

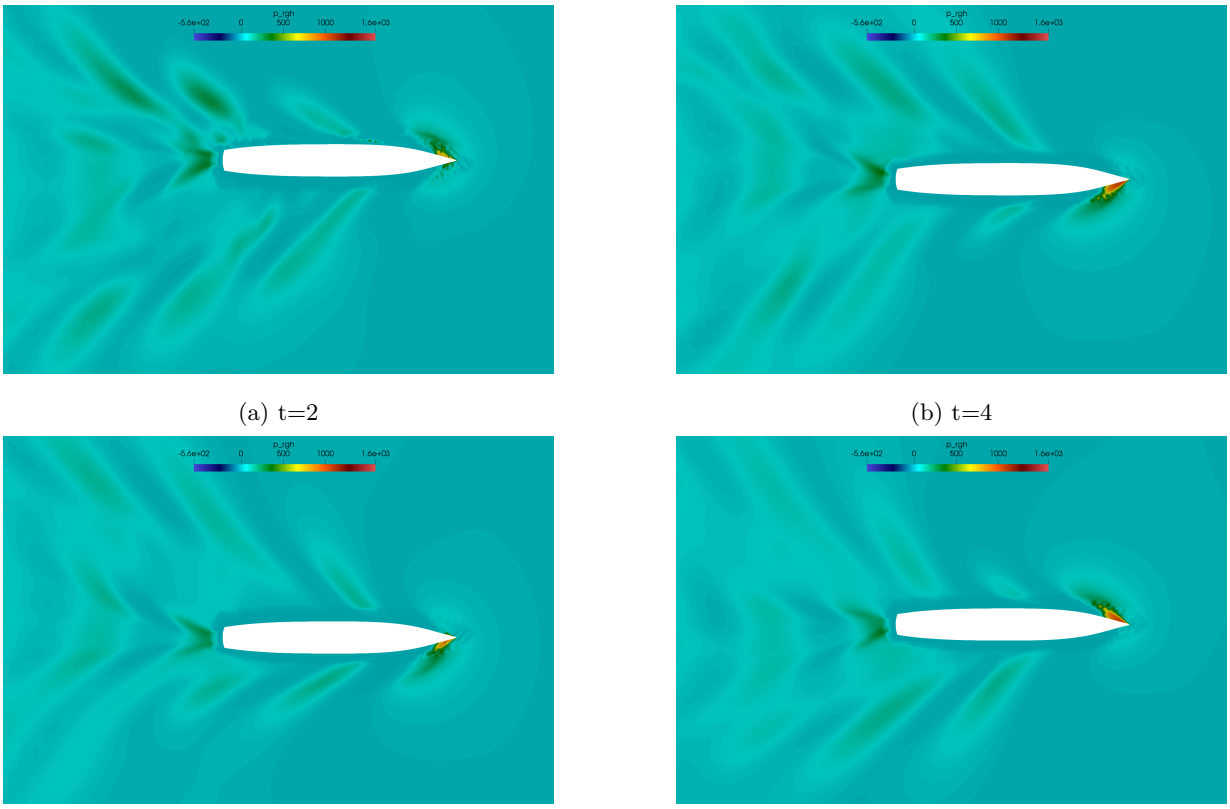

(a) t=2

(b) t=4

(c) t=6

(d) t=8

Figure 3.11: Hydrodynamic pressure distribution on the free surface: pure sway.

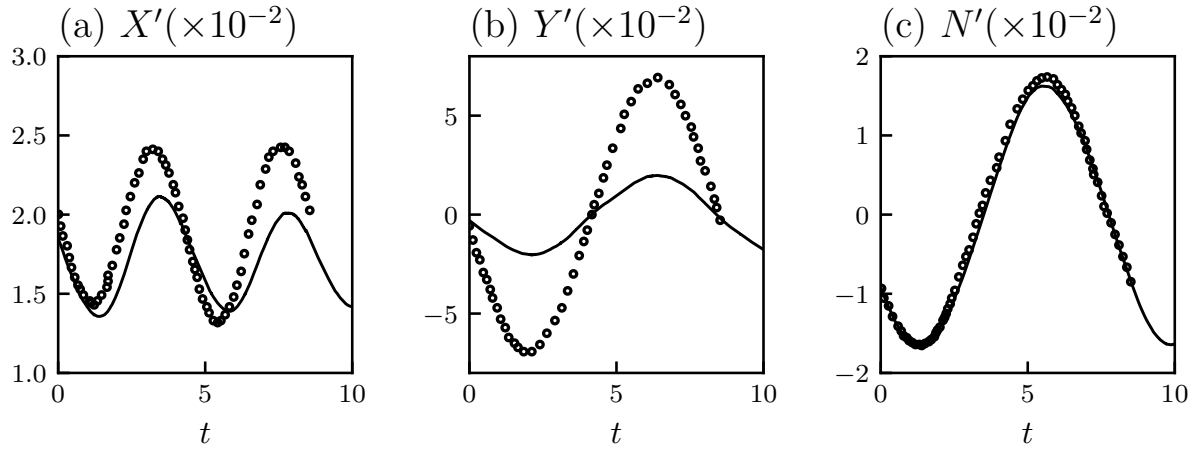

Figure 3.12: Forces and moment coefficient for pure yaw.

lead to a large error when the flow separation occurs at a large drift angle; (3) the non-orthogonality of the deformed grid due to the large magnitude motion of the ship; (4)the hull model without bilge keels in the simulation, compared with the model in the experiment [46].

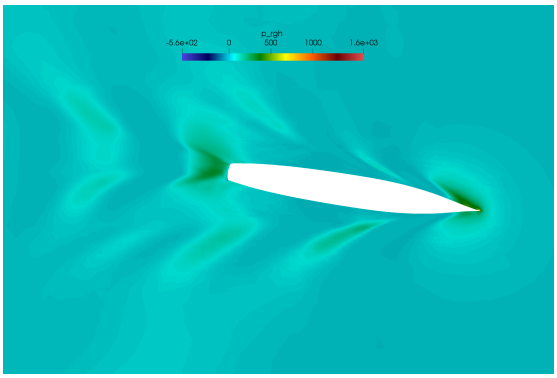

(a) t=7

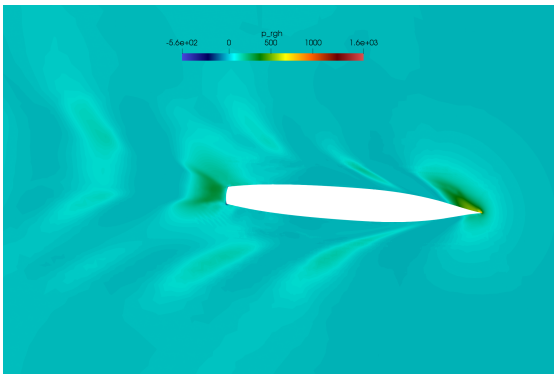

(b) t=8

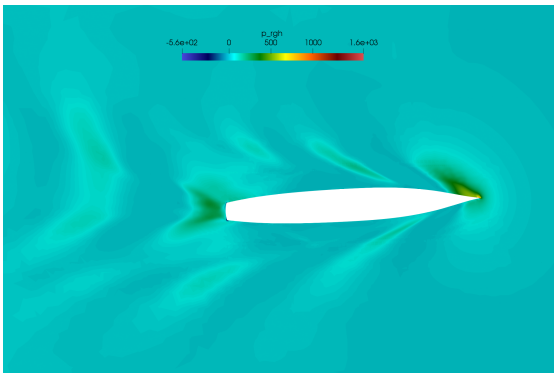

(c) t=9

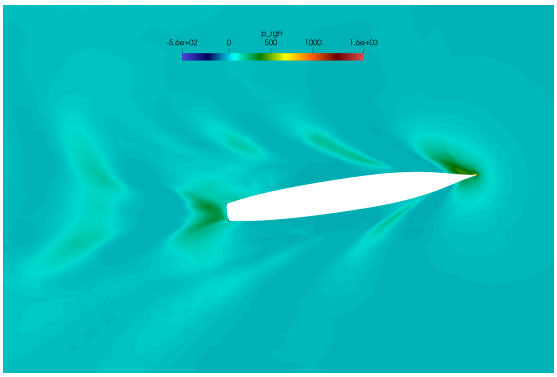

(d) t=10

Figure 3.13: Hydrodynamic pressure distribution on the free surface: pure yaw.

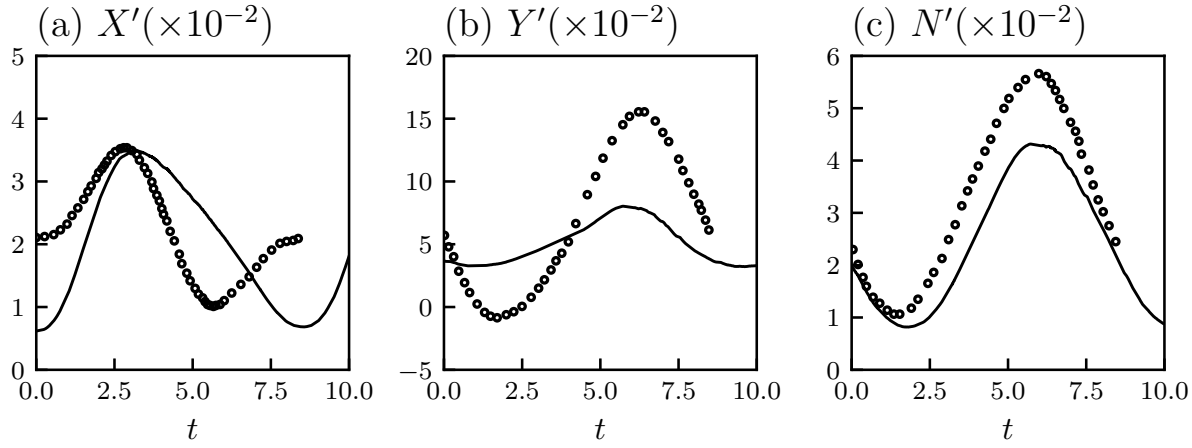

Figure 3.14: Forces and moment coefficient for yaw and drift.

Chapter 4

Conclusions and Future Work

4.1 Conclusions

This report summarizes the main results for the predictive static and dynamic PMM simulations of the force and moment coefficients during ship manoeuvring using the fully open-source software package, OpenFOAM. All the pre- and post-processing steps are conducted using open-source tools. The well-established DTMB 5415 test case is used to benchmark the numerical simulations. Additionally, the DTC test case is simulated to add an additional validation case for the predictive forces and moments. The results present good agreement with experimental data, except three specific cases:

1. at a high Froude number;
2. for large steady drift angled (16° and 20° degree cases);
3. for the specific unsteady yaw rate of 0.3 and drift angle of 10° case.

This report concludes that OpenFOAM is able to solve the forces and moment in ships manoeuvring problems with a good accuracy.

The numerical simulations are done using the InterFoam and InterDyMFoam package within OpenFOAM, which is a turbulent RANS solver using a VOF method to account for the two-phases of the simulation in a continuous regime (without needing to track the discrete air-water interface). The InterFoam solver is used for static drift simulation and dynamic PMM (pure sway, pure yaw, yaw and drift) simulation is performed by the InterDyMFoam solver. The mesh is non-body conforming and generated via successive mesh refinement and adaptation. Dynamic mesh technique is used for dynamic PMM simulation, where the mesh deformed during the ship movement. Despite the lower accuracy of this grid generation method, the results show an overall good agreement with experimental data and published numerical results; all results are presented in a ship-fixed coordinate system.

For steady drift simulation, a time-converged result is obtained to compare with experimental data. At a drift=0°, at various Froude numbers (from 0.174 to 0.218), the relative error of the resistance coefficient for DTC is smaller than 1.6% . For DTMB 5415, the magnitude of relative error increases at large Froude numbers and reaches 12.1% at Fr=0.45, due to the increasing non-dimensional first layer distance to the hull y^+–resulting in a larger near wall resolution error. The insufficient mesh resolution induces larger error for the cases of static drift 16° and 20°, especially for lateral force coefficient.

The unsteady PMM simulations are validated by comparing the converged time-periodic result in the simulation with experiment. Despite much effort, the prediction of pure sway and pure yaw compared less favorably than the steady simulation results. Further investigation is need to improve the prediction result for yaw and drift cases. Different from the experiment by Simonsen [46], there is no bilge keel with the bare hull in the current simulation model, which may lead to the error. The combination effect of lower accuracy mesh generation method and dynamic deformation mesh results in large deviation of unsteady PMM simulation. The overset method is ideal for dynamic PMM simulation; however, currently it is only implemented in commercial software and in some in-house codes by some groups. To implement the overset method in the current OpenFOAM version 17.12 should be considered as the next step of work.

4.2 Future Work

High-quality body fitted mesh by commercial software such as Pointwise should be finished for static cases. For dynamic PMM cases, overset method is needed. On the other hand, modelling requirements including

the mesh resolution criteria and turbulent models for a multiphase ship simulation need to be investigated systematically by decomposing the current multiphase complex ship simulation by some simple benchmark cases. In the current simulation, the forces and moments are integral results, which are influenced by the complex flow phenomena in a ship manoeuvring problem.

References

[1] Inletoutlet boundary condition in OpenFOAM. https://www.cfdsupport.com/OpenFOAM-Training-by-CFD-Support/node114.html. Accessed: 2019-3-30.

[2] OpenCFD release OpenFOAM v1712. https://www.openfoam.com/releases/openfoam-v1712/. Accessed: 2018-12-31.

[3] Tokyo 2015: a workshop on CFD in ship hydrodynamics. https://t2015.nmri.go.jp/announcement.html. Accessed: 2019-3-30.

[4] US navy combatant, DTMB 5415. http://www.simman2008.dk/5415/combatant.html.

[5] L. Benedetti, B. Bouscasse, R. Broglia, L. Fabbri, F. L. Gala, and C. Lugni. PMM model test with DDG51 including uncertainty assessment. *FORCE Technology, Department of Maritime Industry, Lyngby*, 2007.

[6] P.M. Carrica, F. Ismail, M. Hyman, S. Bhushan, and F. Stern. Turn and zigzag maneuvers of a surface combatant using a URANS approach with dynamic overset grids. *Journal of Marine Science and technology*, 18(2):166–181, 2013.

[7] I. B. Celik, U. Ghia, and P.J. Roache. Procedure for estimation and reporting of uncertainty due to discretization in CFD applications. *Journal of Fluids Engineering-Transactions of the ASME*, 130(7), 2008.

[8] O. el Moctar, V. Shigunov, and T. Zorn. Duisburg test case: Post-panamax container ship for benchmarking. *Ship Technology Research*, 59(3):50–64, 2012.

[9] O. el Moctar, F. Sprenger, T. Schellin, and A. Papanikolaou. Numerical and experimental investigations of ship maneuvers in waves. In *ASME 2016 35th International Conference on Ocean, Offshore and Arctic Engineering, Busan, South Korea*, 2016.

[10] J. Gorski, S. Kim, S. Aram, B. Rhee, and H. Shan. Development of a CFD framework for prognoses of resistance, powering, maneuvering, and seakeeping of surface ships. In *30th Symposium of Naval Hydrodynamics*, 2014.

[11] L. Gui, J. Longo, B. Metcalf, J. Shao, and F. Stern. Forces, moment, and wave pattern for surface combatant in regular head waves. Part I. Measurement systems and uncertainty assessment. *Experiments in Fluids*, 31(6):674–680, 2001.

[12] L. Gui, J. Longo, B. Metcalf, J. Shao, and F. Stern. Forces, moment and wave pattern for surface combatant in regular head waves. Part II. Measurement results and discussions. *Experiments in Fluids*, 32(1):27–36, 2002.

[13] R. He, Z.Z. Zhang, X.Z. Wang, and D.K. Feng. Numerical simulation of the ship bottom interaction of DTC container carrier for different keel clearance in pure sway motion. In *4th MASHCON-International Conference on Ship Manoeuvring in Shallow and Confined Water with Special Focus on Ship Bottom Interaction*, pages 65–72, 2016.

[14] C.W. Hirt and B.D. Nichols. Volume of fluid (VOF) method for the dynamics of free boundaries. *Journal of Computational Physics*, 39(1):201–225, 1981.

[15] M. Irvine, J. Longo, and F. Stern. Pitch and heave tests and uncertainty assessment for a surface combatant in regular head waves. *Journal of Ship Research*, 52(2):146–163, 2008.

[16] H. Islam and C.G. Soares. Estimation of hydrodynamic derivatives of a container ship using PMM simulation in OpenFOAM. *Ocean Engineering*, 164:414–425, 2018.

[17] H. Jasak. Dynamic mesh handling in OpenFOAM. In *47th AIAA Aerospace Sciences Meeting Including the New Horizons Forum and Aerospace Exposition*, page 341, 2009.

[18] D.A. Jones and D.B. Clarke. FLUENT code simulation of flow around a naval hull: the DTMB 5415. Technical report, Defence Science and Technology Organization Victoria (Austrilia) Maritime Platforms DIV, 2010.

[19] T. Kawamura and H. Miyata. Simulation of nonlinear ship flows by density-function method. *Journal of The Society of Naval Architects of Japan*, 1994(176):1–10, 1994.

[20] H.C. Kim, H. Akimoto, and H. Islam. Estimation of the hydrodynamic derivatives by RANS simulation of planar motion mechanism test. *Ocean Engineering*, 108:129–139, 2015.

[21] S.E. Kim, B.J. Rhee, and R.W. Miller. Anatomy of turbulent flow around DARPA SUBOFF body in a turning maneuver using high-fidelity RANS computations. *International Shipbuilding Progress*, 60(1-4):207–231, 2013.

[22] S.E. Kim and S. Schroeder. Numerical study of thrust-breakdown due to cavitation on a hydrofoil, a propeller, and a water jet. In *Proceedings of the 28th Symposium on Naval Hydrodynamics, Pasadena, CA*, 2010.

[23] O.K. Kinaci, A. Kukner, and S. Bal. On propeller performance of DTC post-panamax container ship. *International Journal of Ocean System Engineering*, 3(2):77–89, 2013.

[24] L. Larsson, F. Stern, and V. Bertram. Benchmarking of computational fluid dynamics for ship flows: the Gothenburg 2000 workshop. *Journal of Ship Research*, 47(1):63–81, 2003.

[25] L. Larsson, F. Stern, and M. Visonneau. *Numerical ship hydrodynamics: an assessment of the Gothenburg 2010 workshop*. Springer, 2013.

[26] S.K. Lee, J.M. You, H.H. Lee, T. Lim, S.T. Park, J.H. Seo, S.H. Rhee, and K.P. Rhee. Experimental study on the six degree-of-freedom motions of a damaged ship floating in regular waves. *IEEE Journal of Oceanic Engineering*, 41(1):40–49, 2016.

[27] S.K. Lee, J.M. You, H.H Lee, T. Lim, S.H. Rhee, and K.P. Rhee. Preliminary tests of a damaged ship for CFD validation. *International Journal of Naval Architecture and Ocean Engineering*, 4(2):172–181, 2012.

[28] J. Ley, S. Sigmund, and O. el Moctar. Numerical prediction of the added resistance of ships in waves. In *ASME 2014 33rd International Conference on Ocean, Offshore and Arctic Engineering*. American Society of Mechanical Engineers, 2014.

[29] J.L. Liu, R. Hekkenberg, E. Rotteveel, and H. Hopman. Literature review on evaluation and prediction methods of inland vessel manoeuvrability. *Ocean Engineering*, 106:458–471, 2015.

[30] S.K. Liu, A. Papanikolaou, and G. Zaraphonitis. Time domain simulation of nonlinear ship motions using an impulse response function method. In *ICMT conference, July*, 2014.

[31] J. Longo and F. Stern. Resistance, sinkage and trim, wave profile, and nominal wake tests and uncertainty assessment for DTMB model 5512. In *Proc 25th American Towing Tank Conference, Iowa*, 1998.

[32] J. Longo and F. Stern. Uncertainty assessment for towing tank tests with example for surface combatant DTMB model 5415. *Journal of Ship Research*, 49(1):55–68, 2005.

[33] J. Ma and D.C. Wan. A numerical study of resistance and viscous flow around typical benchmark surface ship hull. *Scientia Sinica Physica, Mechanica & Astronomica*, 41(2):178, 2011.

[34] F. Menter. Zonal two equation $k\omega$ turbulence models for aerodynamic flows. In *23rd Fluid Dynamics, Plasma Dynamics, and Lasers Conference*, page 2906, 1993.

[35] F. Menter, M. Kuntz, and R. Langtry. Ten years of industrial experience with the SST turbulence model. *Turbulence, Heat and Mass Transfer*, 4(1):625–632, 2003.

[36] C. Oldfield, M.M. Larmaei, A. Kendrick, and K. McTaggart. Prediction of warship manoeuvring coefficients using CFD. In *World Maritime Technology Conference*, 2015.

[37] A. Olivieri, F. Pistani, A. Avanzini, F. Stern, and R. Penna. Towing tank experiments of resistance, sinkage and trim, boundary layer, wake, and free surface flow around a naval combatant INSEAN 2340 model. Technical report, Iowa Univ Iowa City Coll of Engineering, 2001.

[38] H. Orihara and H. Miyata. Evaluation of added resistance in regular incident waves by computational fluid dynamics motion simulation using an overlapping grid system. *Journal of Marine Science and Technology*, 8(2):47–60, 2003.

[39] H.P. Piehl. *Ship roll damping analysis*. PhD thesis, University of Duisburg Essen, 2016.

[40] I.-R. Procedures. Practical guidelines for ship CFD applications. *In Guidelines 2011; 26th ITTC Specialist Committee on CFD in Marine Hydrodynamics; Lyngby, Denmark*, pages 1–18, 2011.

[41] N. Sakamoto, P.M. Carrica, and F. Stern. URANS simulations of static and dynamic maneuvering for surface combatant: part 1. verification and validation for forces, moment, and hydrodynamic derivatives. *Journal of Marine Science and Technology*, 17(4):422–445, 2012.

[42] Z.R. Shen. *Development of overset grid technique for hull-propeller-rudder interactions*. PhD thesis, Shanghai Jiao Tong University, 2014.

[43] Z.R. Shen and D.C. Wan. RANS computations of added resistance and motions of a ship in head waves. *International Journal of Offshore and Polar Engineering*, 23(04):264–271, 2013.

[44] Z.R. Shen, D.C. Wan, and P.M. Carrica. RANS simulations of free maneuvers with moving rudders and propellers using overset grids in OpenFOAM. In *SIMMAN workshop on Verification and Validation of Ship Maneuvering Simulation Methods. Presented at the SIMMAN workshop on Verification and Validation of Ship Maneuvering Simulation Methods, Lyngby, Denmark*, 2014.

[45] Z.R. Shen, D.C. Wan, and P.M. Carrica. Dynamic overset grids in OpenFOAM with application to KCS self-propulsion and maneuvering. *Ocean Engineering*, 108:287–306, 2015.

[46] C.D. Simonsen. PMM model test with DDG51 including uncertainty assessment. *FORCE Technology, Department of Maritime Industry, Lyngby*, 2004.

[47] F. Stern, J. Longo, R. Penna, A. Olivieri, T. Ratcliffe, and H. Coleman. International collaboration on benchmark CFD validation data for surface combatant DTMB model 5415. In *Twenty-Third Symposium on Naval Hydrodynamics Office of Naval Research Bassin d'Essais des Carenes National Research Council*, 2001.

[48] F. Stern, J.M. Yang, Z.Y. Wang, H.S. Hosseini, M. Mousaviraad, S. Bhushan, and T. Xing. Computational ship hydrodynamics: nowadays and way forward. *International Shipbuilding Progress*, 60(1-4):3–105, 2013.

[49] M. Terziev, T. Tezdogan, E. Oguz, T. Gourlay, Y.K. Demirel, and A. Incecik. Numerical investigation of the behaviour and performance of ships advancing through restricted shallow waters. *Journal of Fluids and Structures*, 76:185–215, 2018.

[50] S.L. Toxopeus. *Practical application of viscous-flow calculations for the simulation of manoeuvring ships*. PhD thesis, Technische Universiteit Delft, 2011.

[51] V. Vukcevic, A. Ostman, and H. Jasak. Rapid simulations of pure sway motion using FVM in OpenFOAM. In *Proceedings of workshop on verification and validation of ship manoeuvring simulation methods (SIMMAN 2014)*, 2014.

[52] J.H. Wang and D.C. Wan. Numerical simulation of pure yaw motion using dynamic overset grid technology. *Chinese Journal of Hydrodynamics*, 31(5):567–574, 2016.

[53] M.P. Wood, L.M. González, J. Izquierdo, A. Sarasquete, and L.P. Rojas. RANSE with free surface computations around fixed DTMB 5415 model and other baliños fishing vessels. In *9th International Conference on Numerical Ship Hydrodynamics, Michigan, USA*, pages 5–8, 2007.

[54] H.S. Yoon. *Phase-averaged stereo-PIV flow field and force/moment/motion measurements for surface combatant in PMM maneuvers*. PhD thesis, University of Iowa, 2009.

[55] H.S. Yoon, C.D. Simonsen, L. Benedetti, J. Longo, Y. Toda, and F. Stern. Benchmark CFD validation data for surface combatant 5415 in PMM maneuvers. Part I: Force/moment/motion measurements. *Ocean Engineering*, 109:705–734, 2015.

APPENDICES

Appendix A

Configuration file for pure drift simulation in OpenFOAM

A.1 Allrun

```
#!/bin/sh
cd ${0%/*} || exit 1                        # Run from this directory
. $WM_PROJECT_DIR/bin/tools/RunFunctions    # Tutorial run functions
# copy DTC hull surface from resources folder
\cp DTM-MARIN-yaw0roll0.stl  constant/triSurface/DTM.stl
runApplication surfaceFeatureExtract
runApplication blockMesh
#for i in 1 2 3 4  5 6
#do
#    runApplication -s $i \
#        topoSet -dict system/topoSetDict.${i}

#    runApplication -s $i \
#        refineMesh -dict system/refineMeshDict -overwrite
#done
runApplication decomposePar
runParallel  snappyHexMesh -overwrite
#restore0Dir
ls -d processor* | xargs -I {} rm -rf ./{}/0
ls -d processor* | xargs -I {} cp -r 0.orig ./{}/0
runParallel  setFields
```

```
#runApplication decomposePar
runParallel patchSummary
runParallel $(getApplication)
runApplication reconstructParMesh -constant
runApplication reconstructPar  #-latestTime
runApplication foamToVTK
```

A.2 system/controlDict

```
FoamFile
{
    version     2.0;
    format      ascii;
    class       dictionary;
    location    "system";
    object      controlDict;
}
application     interFoam;
startFrom       latestTime; //startTime;
startTime       0;
stopAt          endTime;
endTime         4000;
deltaT          1;
writeControl    timeStep;
writeInterval   200;
purgeWrite      0;
writeFormat     binary;
writePrecision  6;
writeCompression off;
timeFormat      general;
timePrecision   6;
runTimeModifiable yes;
functions
{
    forces
    {
        type            forces;
        libs            ("libforces.so");
        patches         (hull);
        rhoInf          998.8;
        log             on;
        writeControl    timeStep;
        writeInterval   1;
        CofR            (2 0 0.18);
    }
    #includeFunc Q
    #include "surfaces"
```

```
}
```

A.3 system/blockMeshDict

```
FoamFile
{
    version     2.0;
    format      ascii;
    class       dictionary;
    object      blockMeshDict;
}
scale   1;
vertices
(
    (-18 -9 -6)
    (12 -9 -6)
    (12 9 -6)
    (-18 9 -6)
    (-18 -9 1)
    (12 -9 1)
    (12 9 1)
    (-18 9 1)
);
//Lx=40, Ly=18,Lz=9
//dx=dy=dz=0.0
//(20% y-dir, 30% cells, last mesh/first mesh = 1/35=0.02857 )
blocks
(
    hex (0 1 2 3 4 5 6 7) (140 50 26)
    simpleGrading
    (((17 20 0.033333)(8 80 1) (5 13 8.5))
    ((8.5 16 0.0714) (1 10 1) (8.5 16 14))
    ((5.8 14 0.1) (1.2 12 1)))
);

edges
(
);

boundary
(
    atmosphere
    {
        type patch;
        faces
        (
```

```
            (4 5 6 7)
        );
    }
    inlet
    {
        type patch;
        faces
        (
            (1 2 6 5)
        );
    }
    outlet
    {
        type patch;
        faces
        (
            (0 4 7 3)
        );
    }
    bottom
    {
        type symmetryPlane;
        faces
        (
            (0 3 2 1)
        );
    }
    side
    {
        type patch;
        faces
        (
            (0 1 5 4)
        );
    }
    midPlane
    {
        type patch;
        faces
        (
            (3 7 6 2)
        );
    }
);
mergePatchPairs
(
);
```

A.4 system/fvSchemes

```
FoamFile
{
    version     2.0;
    format      ascii;
    class       dictionary;
    location    "system";
    object      fvSchemes;
}
ddtSchemes
{
    default         localEuler;
}

gradSchemes
{
    default         Gauss linear;
    limitedGrad     cellLimited Gauss linear 1;
}

divSchemes
{
    div(rhoPhi,U)   Gauss linearUpwind grad(U);
    div(phi,alpha)  Gauss vanLeer;
    div(phirb,alpha) Gauss linear;
    div(phi,k)      Gauss linearUpwind limitedGrad;
    div(phi,omega)  Gauss linearUpwind limitedGrad;
    div(((rho*nuEff)*dev2(T(grad(U))))) Gauss linear;
}
laplacianSchemes
{
    default         Gauss linear corrected;
}
interpolationSchemes
{
    default         linear;
}
snGradSchemes
{
    default         corrected;
}
wallDist
{
    method meshWave;
}
```

A.5 system/fvSolution

```
FoamFile
{
    version     2.0;
    format      ascii;
    class       dictionary;
    location    "system";
    object      fvSolution;
}
solvers
{
    "alpha.water.*"
    {
        nAlphaCorr      2;
        nAlphaSubCycles 1;
        cAlpha          1;
        icAlpha         0;
        MULESCorr       yes;
        nLimiterIter    10;
        alphaApplyPrevCorr  yes;
        solver          smoothSolver;
        smoother        symGaussSeidel;
        tolerance       1e-8;
        relTol          0;
        minIter         1;
    }

    "pcorr.*"
    {
        solver          PCG;
        preconditioner
        {
            preconditioner  GAMG;
            smoother        GaussSeidel;
            tolerance       1e-5;
            relTol          0;
        };

        tolerance       1e-5;
        relTol          0;
    };

    p_rgh
    {
        solver          GAMG;
        smoother        DIC;
        tolerance       1e-7;
        relTol          0.01;
```

```
    };

    p_rghFinal
    {
        $p_rgh;
        relTol          0;
    }

    "(U|k|omega).*"
    {
        solver          smoothSolver;
        smoother        symGaussSeidel;
        nSweeps         1;
        tolerance       1e-7;
        relTol          0.1;
        minIter         1;
    };
}

PIMPLE
{
    momentumPredictor   no;
    nOuterCorrectors    1;
    nCorrectors         2;
    nNonOrthogonalCorrectors 0;
    maxCo               10;
    maxAlphaCo          5;
    rDeltaTSmoothingCoeff 0.05;
    rDeltaTDampingCoeff 0.5;
    nAlphaSpreadIter    0;
    nAlphaSweepIter     0;
    maxDeltaT           1;
}
relaxationFactors
{
    equations
    {
        ".*" 1;
    }
}
cache
{
    grad(U);
}
```

A.6 system/decomposeParDict

```
FoamFile
```

```
{
    version     2.0;
    format      ascii;
    class       dictionary;
    object      decomposeParDict;
}
numberOfSubdomains 40;
method          scotch;
coeffs
{
    n           (4 5 2);
    //delta       0.001; // default=0.001
    //order       xyz;   // default=xzy
}
distributed     no;
roots
(
);
```

A.7 system/snappyHexMeshDict

```
FoamFile
{
    version     2.0;
    format      ascii;
    class       dictionary;
    object      snappyHexMeshDict;
}
// Which of the steps to run
castellatedMesh true;
snap            true;
//addLayers       true;
addLayers false;
geometry
{
    DTM.stl
    {
        type triSurfaceMesh;
        name hull;
        patchInfo
        {
            type wall;
        }
    }
    refinementBox
    {
        type    searchableBox;
```

```
        min     (-18 -9 -0.4);
        max     ( 12  9  0.6);
    }
};
// Settings for the castellatedMesh generation.
castellatedMeshControls
{
    maxLocalCells 1000000;
    maxGlobalCells 20000000;
    minRefinementCells 0;
    nCellsBetweenLevels 6;
    features
    (
         {
             file "DTM.eMesh";
             level 0;
         }
    );
refinementSurfaces
    {
        hull
        {
            // Surface-wise min and max refinement level
            level (3 3);
        }
    }
    resolveFeatureAngle 45;
    refinementRegions
    {
        refinementBox
        {
            mode inside;
            levels ((1e15 1));
        }
    }
    locationInMesh (-0.7 0 0);
    allowFreeStandingZoneFaces true;
}
// Settings for the snapping.
snapControls
{
    nSmoothPatch 3;
    tolerance 4.0;
    nSolveIter 100;
    nRelaxIter 5;
    nFeatureSnapIter 10;
}
// Settings for the layer addition.
addLayersControls
{
```

```
    layers
    {
        hull
        {
            nSurfaceLayers 6;
        }
    }
    // Expansion factor for layer mesh
    expansionRatio 1.5;
    finalLayerThickness 0.7;
    minThickness 0.25;
    nGrow 0;
    featureAngle 60;
    nRelaxIter 5;
    nSmoothSurfaceNormals 1;
    nSmoothNormals 3;
    nSmoothThickness 10;
    maxFaceThicknessRatio 0.5;
    maxThicknessToMedialRatio 0.3;
    minMedianAxisAngle 90;
    nBufferCellsNoExtrude 0;
    nLayerIter 50;
    nRelaxedIter 20;
}
meshQualityControls
{
    #include "meshQualityDict"
}
mergeTolerance 1E-6;
```

A.8 0.orig/U

```
FoamFile
{
    version     2.0;
    format      ascii;
    class       volVectorField;
    location    "0";
    object      U;
}
//Umean   1.75405221724;      // In order for Fr = 0.28
//mUmean -1.75405221724;
//theta=10
//U-X=U*cos(theta)=-1.727404223
//U-y=U*sin(theta)=-0.304587971
dimensions      [0 1 -1 0 0 0 0];
//internalField   uniform ($mUmean 0 0);
```

```
internalField   uniform (-1.727404223 -0.304587971 0);
boundaryField
{
    #includeEtc "caseDicts/setConstraintTypes"
//inlet
    inlet
    {
        type            fixedValue;
        value           $internalField;
    }
midPlane
    {
        type            fixedValue;
        value           $internalField;
    }
//outlet
    outlet
    {
        type            zeroGradient;
    }
    side
    {
        type            zeroGradient;
    }
    atmosphere
    {
        type            pressureInletOutletVelocity;
        value           uniform (0 0 0);
    }
    hull
    {
        type            movingWallVelocity;
        value           uniform (0 0 0);
    }
}
```

A.9 0.orig/p-rgh

```
FoamFile
{
    version     2.0;
    format      ascii;
    class       volScalarField;
    location    "0";
    object      p_rgh;
}
dimensions      [1 -1 -2 0 0 0 0];
```

```
internalField   uniform 0;
boundaryField
{
    #includeEtc "caseDicts/setConstraintTypes"
//inlet
    inlet
    {
        type            fixedFluxPressure;
        value           $internalField;
    }
//add 2018.8.13
midPlane
    {
        type            fixedFluxPressure;
        value           $internalField;
    }
//outlet
    outlet
    {
        type            zeroGradient;
    }

side
    {
        type            zeroGradient;
    }
    atmosphere
    {
        type            totalPressure;
        p0              uniform 0;
    }
    hull
    {
        type            fixedFluxPressure;
        value           $internalField;
    }
}
```

A.10 0.orig/alpha.water

```
FoamFile
{
    version     2.0;
    format      ascii;
    class       volScalarField;
    location    "0";
    object      alpha;
```

```
}
dimensions      [0 0 0 0 0 0 0];
internalField   uniform 0;
boundaryField
{
    #includeEtc "caseDicts/setConstraintTypes"
//inlet
    inlet
    {
        type            fixedValue;
        value           $internalField;
    }
midPlane
    {
        type            fixedValue;
        value           $internalField;
    }
//outlet
    outlet
    {
        type            variableHeightFlowRate;
        lowerBound      0;
        upperBound      1;
        value           $internalField;
    }
side
    {
        type            variableHeightFlowRate;
        lowerBound      0;
        upperBound      1;
        value           $internalField;
    }
    atmosphere
    {
        type            inletOutlet;
        inletValue      $internalField;
        value           $internalField;
    }
    hull
    {
        type            zeroGradient;
    }
}
```

A.11 0.orig/omega

```
FoamFile
```

```
{
    version     2.0;
    format      ascii;
    class       volScalarField;
    location    "0";
    object      omega;
}
dimensions      [0 0 -1 0 0 0 0];
internalField   uniform 2;
boundaryField
{
    #includeEtc "caseDicts/setConstraintTypes"
//inlet
    inlet
    {
        type            fixedValue;
        value           $internalField;
    }
midPlane
    {
        type            fixedValue;
        value           $internalField;
    }
//outlet
    outlet
    {
       type            inletOutlet;
       inletValue      $internalField;
       value           $internalField;
    }
side
    {
       type            inletOutlet;
       inletValue      $internalField;
       value           $internalField;
    }
    atmosphere
    {
        type            inletOutlet;
        inletValue      $internalField;
        value           $internalField;
    }
    hull
    {
        type            omegaWallFunction;
        value           $internalField;
    }
}
```

A.12 0.orig/k

```
FoamFile
{
    version     2.0;
    format      ascii;
    class       volScalarField;
    location    "0";
    object      k;
}
dimensions      [0 2 -2 0 0 0 0];
internalField   uniform 0.00015;
boundaryField
{
    #includeEtc "caseDicts/setConstraintTypes"
    inlet
    {
        type            fixedValue;
        value           $internalField;
    }
    midPlane
    {
        type            fixedValue;
        value           $internalField;
    }
    outlet
    {
       type            inletOutlet;
       inletValue      $internalField;
       value           $internalField;
    }
side
    {
       type            inletOutlet;
       inletValue      $internalField;
       value           $internalField;
    }
    atmosphere
    {
        type            inletOutlet;
        inletValue      $internalField;
        value           $internalField;
    }
    hull
    {
        type            kqRWallFunction;
        value           $internalField;
    }
}
```

A.13 0.orig/nut

```
FoamFile
{
    version     2.0;
    format      ascii;
    class       volScalarField;
    location    "0";
    object      nut;
}
dimensions      [0 2 -1 0 0 0 0];
internalField   uniform 5e-07;
boundaryField
{
    #includeEtc "caseDicts/setConstraintTypes"
//inlet
    inlet
    {
        type            fixedValue;
        value           $internalField;
    }
    midPlane
    {
        type            fixedValue;
        value           $internalField;
    }
//outlet
    outlet
    {
        type            zeroGradient;
    }
side
    {
        type            zeroGradient;
    }
    atmosphere
    {
        type            zeroGradient;
    }
    hull
    {
        type            nutkRoughWallFunction;
        Ks              uniform 100e-6;
        Cs              uniform 0.5;
        value           $internalField;
    }
}
```

A.14 constant/turbulenceProperties

```
FoamFile
{
    version     2.0;
    format      ascii;
    class       dictionary;
    location    "constant";
    object      turbulenceProperties;
}
simulationType  RAS;
RAS
{
    RASModel        kOmegaSST;
    turbulence      on;
    printCoeffs     on;
}
```

A.15 constant/transportProperties

```
FoamFile
{
    version     2.0;
    format      ascii;
    class       dictionary;
    location    "constant";
    object      transportProperties;
}
phases (water air);
water
{
    transportModel  Newtonian;
    nu              1.09e-06;
    rho             998.8;
}
air
{
    transportModel  Newtonian;
    nu              1.48e-05;
    rho             1;
}
sigma           0;
```

A.16 constant/hRef

```
FoamFile
{
    version     2.0;
    format      ascii;
    class       uniformDimensionedScalarField;
    location    "constant";
    object      hRef;
}
dimensions      [0 1 0 0 0 0 0];
value           0.178941; // STL already lowered
```

A.17 constant/g

```
FoamFile
{
    version     2.0;
    format      ascii;
    class       uniformDimensionedVectorField;
    location    "constant";
    object      g;
}
dimensions      [0 1 -2 0 0 0 0];
value           (0 0 -9.806); // according to Oldfield et. al.
```

DOCUMENT CONTROL DATA

*Security markings for the title, authors, abstract and keywords must be entered when the document is sensitive

1. ORIGINATOR (Name and address of the organization preparing the document. A DRDC Centre sponsoring a contractor's report, or tasking agency, is entered in Section 8.)

Department of Mechanical and Mechatronics Engineering, University of Waterloo,
200 University Ave W, Waterloo, Ontario, Canada, N2L 3G1

Department of Mechanical and Aerospace Engineering, Royal Military College of Canada
13 General Crerar Crescent, Kingston, Ontario, Canada, K7K 7B4

2a. SECURITY MARKING (Overall security marking of the document including special supplemental markings if applicable.)

CAN UNCLASSIFIED

2b. CONTROLLED GOODS

NON-CONTROLLED GOODS
DMC A

3. TITLE (The document title and sub-title as indicated on the title page.)

Prediction of Warship Manoeuvring Coefficients using OpenFOAM

4. AUTHORS (Last name, followed by initials – ranks, titles, etc., not to be used)

Liu, C.; Sia, J.; Hickey, J.-P.; Wu, X.

5. DATE OF PUBLICATION (Month and year of publication of document.)	6a. NO. OF PAGES (Total pages, including Annexes, excluding DCD, covering and verso pages.)	6b. NO. OF REFS (Total references cited.)
October 2019	72	55

7. DOCUMENT CATEGORY (e.g., Scientific Report, Contract Report, Scientific Letter.)

Contract Report

8. SPONSORING CENTRE (The name and address of the department project office or laboratory sponsoring the research and development.)

DRDC – Atlantic Research Centre
Defence Research and Development Canada
9 Grove Street
P.O. Box 1012
Dartmouth, Nova Scotia B2Y 3Z7
Canada

9a. PROJECT OR GRANT NO. (If appropriate, the applicable research and development project or grant number under which the document was written. Please specify whether project or grant.)	9b. CONTRACT NO. (If appropriate, the applicable number under which the document was written.)
01ef - More Navy	PA16004; DND RMCC - Service Level Arrangement with Royal Military College of Canada (RMCC) concerning contribution to DRDC's Program

10a. DRDC PUBLICATION NUMBER (The official document number by which the document is identified by the originating activity. This number must be unique to this document.)	10b. OTHER DOCUMENT NO(s). (Any other numbers which may be assigned this document either by the originator or by the sponsor.)
DRDC-RDDC-2019-C259	

11a. FUTURE DISTRIBUTION WITHIN CANADA (Approval for further dissemination of the document. Security classification must also be considered.)

Public release

11b. FUTURE DISTRIBUTION OUTSIDE CANADA (Approval for further dissemination of the document. Security classification must also be considered.)

12. KEYWORDS, DESCRIPTORS or IDENTIFIERS (Use semi-colon as a delimiter.)

Computational Fluid Dynamics (CFD); Maneuvering; Naval Architecture

13. ABSTRACT/RÉSUMÉ (When available in the document, the French version of the abstract must be included here.)

This report summarizes the results for the static and dynamic planar motion mechanism (PMM) simulations of ship manoeuvring using the open-source Computational Fluid Dynamics software package, OpenFOAM. The well-established DTMB 5415 test case is used to benchmark the static and dynamic PMM simulations. Additionally, the static drift DTC test case is presented as an additional validation case for the predictive force and moment coefficients. The numerical simulations are performed using the InterFoam (for static case) and InterDyMFoam (for dynamic case) packages which are multiphysics CFD solvers based on the volume of fluid (VOF) method to account for the multiple phases in a continuous regime (without needing to track the discrete air-water interface); the turbulence is modelled using Reynolds Averaged Navier Stokes (RANS) approximations. The mesh is non-body conforming and generated via successive mesh refinement and adaptation using open-source software; a dynamic mesh technique is used for dynamic PMM simulations. Despite the lower accuracy of this grid generation method and the mesh deformation in dynamic PMM simulation, the results show an overall good agreement with experimental data and published numerical results. The relative errors remain small—for most of the steady cases under consideration—after a grid convergence study. There are three specific cases in which the error is significant: (1) at a high Froude number; (2) for large steady drift angled (16◦and 20◦degree cases); (3) for the specific unsteady yaw rate of 0.3 and drift angle of 10◦case. In conclusion, OpenFOAM is capable of predicting force and moment coefficients for static and dynamic PMM simulation with a good accuracy outside the three specific cases when the error is non-negligible.

Ce rapport résume les résultats de simulations statiques et dynamiques du mécanisme de mouvement planaire (MMP) des manœuvres d'un navire à l'aide du logiciel OpenFOAM (OpenSource Computational Fluid Dynamics). Le scénario d'essai bien établi DTMB 5415 est utilisé pour étalonner les simulations statiques et dynamiques du MMP. De plus, le scénario d'essai de dérive statique DTC est présenté comme un cas de validation supplémentaire pour les coefficients de force et de moment prédictifs. Les simulations numériques sont effectuées à l'aide des logiciels InterFoam (pour le cas statique) et InterDyMFoam (pour le cas dynamique), qui sont des solveurs CFD multiphysiques basés sur la méthode du volume de fluide (VOF) afin de tenir compte des multiples phases dans un régime continu (sans avoir à suivre l'interface air/eau). La turbulence est modélisée en utilisant des approximations RANS (équations de Navier-Stokes moyennées). Le maillage n'est pas conforme au corps et il est généré par raffinement et adaptation successifs du maillage à l'aide d'un logiciel de source libre. Une technique de maillage dynamique est utilisée pour les simulations MMP dynamiques. Malgré la précision moindre de cette méthode de génération de maillage et la déformation du maillage dans la simulation MMP dynamique, les résultats montrent une bonne concordance globale avec les données expérimentales et les résultats numériques publiés. Après une étude de convergence de maillage, les erreurs relatives restent faibles pour la plupart des cas constants à l'étude. Il y a trois cas spécifiques pour lesquels l'erreur est significative : 1) avec un nombre de Froude élevé, 2) pour les grands angles de dérive stables (16 degrés et 20 degrés), 3) pour une vitesse en lacet instationnaire spécifique de 0,3 et un angle de dérive de 10 degrés. En conclusion, OpenFOAM est capable de prédire les coefficients de force et de moment pour les simulations MMP statique et dynamique avec une bonne précision en dehors des trois cas spécifiques où l'erreur est non négligeable.